Metabolomics insight into the gut microbiome of infants with cow's milk allergy

Zhu, P.

Chapter III

Matrix effects in untargeted LC-MS metabolomics: from creation to compensation with post-column infusion of standards

Based on:

Pingping Zhu, Amy Harms, Pascal Maas, Manisha Bakas, Julia Josette Whien, Anne-Charlotte Dubbelman, Thomas Hankemeier

Matrix Effects in Untargeted LC-MS Metabolomics: From Creation to Compensation with Post-Column Infusion of Standards

Journal of Chromatography A

DOI: 10.1016/j.chroma.2025.466508

Abstract

Matrix effect is a well-known issue affecting accuracy and repeatability in metabolomics studies using liquid chromatography-electrospray ionization-mass spectrometry (LC-ESI-MS). Post-column infusion of standards (PCIS) is a promising strategy to monitor and correct matrix effect but has been rarely reported in untargeted metabolomics. The major challenges lie in selecting appropriate PCISs and identifying the most suitable PCIS to correct the matrix effect experienced by each feature. In this study, we aim to present a method for selecting suitable PCISs for matrix effect compensation based on the artificial matrix effect (ME_{art}) created by post-column infusion of compounds that disrupt the ESI process. Our hypothesis is that the suitable PCIS for a given analyte can be identified by comparing the PCISs' ability in ME_{art} compensation. We evaluated this approach using 19 stable-isotopically labeled (SIL) standards spiked in plasma, urine, and feces. PCISs selected based on ME_{art} were compared to those selected by biological matrix effect (ME_{bio}), with 17 out of 19 SIL standards (89%) showing consistent PCIS selection, demonstrating the effectiveness of ME_{art} in identifying suitable PCISs. Applying ME_{art}-selected PCISs to correct for the ME_{bio} resulted in improved ME_{bio} for most of the SILs affected by matrix effect and maintained ME_{bio} for those experiencing no matrix effect. We demonstrated the efficacy of ME_{art} in selecting suitable PCISs for ME_{bio} correction within an LC-PCIS-MS method. Importantly, since ME_{art} can be assessed for any detected feature, its application holds great potential for identifying suitable PCISs for matrix effect correction in untargeted metabolomics.

1. Introduction

Matrix effect (ME), primarily caused by coeluting matrix components, poses a significant challenge in liquid chromatography-electrospray ionization-mass spectrometry (LC−ESI−MS). It can alter analytes' ionization efficiency through ion suppression or enhancement, affecting the accuracy and reliability of their quantification.[1,2] ME is categorized as absolute matrix effect (AME) and relative matrix effect (RME). AME describes the response differences of an analyte spiked in a biological sample *vs.* a matrix-free sample. RME is defined as the relative standard deviation (RSD%) of the AME among biological samples from different sources, indicating the sample to sample variation.[3] To mitigate ME, strategies such as extensive sample preparation, sample dilution, and tailored LC separation have been employed.[4] The most common method for evaluating ME is post-extraction spiking (PES) of an analyte or its analogue into biological and matrix-free sample and comparing their responses, which is widely applied in targeted metabolomics.[2] For ME correction, an efficient approach is spiking surrogate analytes or internal standards, typically stable isotopically labeled (SIL) standards, into a study sample, then correct the signal of an analyte by that of a surrogate or SIL standard.[5] Although these approaches are effective for ME evaluation and compensation, their application can be limited by high cost and limited commercial availability of analyte analogues and SIL standards.[4,5] Besides, even deuterium-labeled standards can exhibit retention time shifts compared to the analytes due to altered physicochemical properties, which reduces the efficiency of ME correction.[6,7]

The disadvantages of PES and SIL standards spiking can be mitigated by another technique used for addressing ME in LC-MS-based metabolomics: post-column infusion of standard (PCIS). Unlike PES and SIL standards spiking, which assess and correct ME at specific retention times, PCIS allows for ME evaluation and compensation across the entire chromatographic profile by constantly infusing one or several standards into the LC-MS post-column.[1,2] In 1999, PCIS was introduced to monitor ME in plasma samples,[8] and to correct ME in environmental samples.[9] In PCIS, ME can be evaluated or monitored by comparing the signals of an infused standard

between the injections of matrix and solvent samples.[8] Meanwhile, correction can be achieved by normalizing the analyte signal to the signal of a PCIS in a matrix sample.[9] PCIS has proven effective for monitoring or correcting ME in various targeted LC-MS based studies. Applications include quantifying pharmaceuticals in waste water,[10,11] chicken meat,[12] human urine,[11,13–15] human plasma,[11,16] and dry blood spots samples;[17,18] targeting pesticides in food extracts;[19] analyzing steroids,[20] amino acids,[21–23] phospholipids,[24] and other endogenous metabolites. In most of these studies, a structural analogue of the analyte or a single SIL standard is used as the infused standard, which significantly reduces costs compared to using multiple SIL standards. Importantly, different from PES and SIL standards spiking, which are restricted to targeted metabolomics, PCIS is also applicable in untargeted metabolomics due to its independence from retention time.

Although PCIS has been recommended as a quality control tool for ME evaluation in untargeted analysis,[26] its actual use remains limited. Tisler *et al.* demonstrated that PCIS is a suitable approach for correcting the RME of waste water in untargeted profiling.[27] Our recent study showed that PCIS can efficiently monitor the ME in human plasma and fecal samples in untargeted metabolomics.[28] One of the primary obstacle limiting the implementation of PCIS in untargeted metabolomics probably lies in selecting suitable PCIS candidates for diverse metabolome features. The similarity of hydrophobicity and ionization ability between the analytes and PCIS are important factors for efficient ME correction.[13] However, pre-selecting PCIS candidates for all the detected features in untargeted metabolomics according to the physical-chemical properties is impractical, particularly for the unknown ones. This highlights the necessity of physical-chemical diversity in PCIS candidates applied in untargeted metabolomics. Tisler *et al.* evaluated the diversity of six PCISs by examining the variation of their monitored ME. They concluded that the ME consists of retention-time dependent ME and structural-specific ME.[27] Retention-time dependent matrix were compensated using the median value of the ME obtained with all PCISs, while structure-specific ME were addressed with a quantitative structure-property relationships (QSPR) model.[27] Nevertheless, the QSPR model is target dependent, as it requires the physical-chemical property of a compound to predict the structure-specific ME.[27] Thus, an ideal

approach that considers both co-eluting matrix compounds and structure diversities is still lacking for applying PCIS to correct ME in untargeted metabolomics. Instead of using the median ME obtained from several PCISs, matching each feature to its suitable PCIS could help to address the issue of structure diversity. However, this raises another challenge for implementing PCIS to compensate for ME in untargeted metabolomics: how to match a detected feature to its appropriate PCIS?

In this study, we aim to develop a novel methodology for PCIS matching in an LC-PCIS-MS-based untargeted metabolomics method. To achieve this, we first discussed key factors, including concentration optimization and diversity evaluation, for selecting PCIS candidates. Then, a post-column artificial matrix infusion approach was introduced to the developed LC-PCIS-MS method for PCIS matching. The artificial matrices consist of compounds that disrupt the ionization process in the ESI source. Therefore, by comparing the signals of an analyte with and without artificial matrix infusion, its artificial ME (ME_{art}) can be determined. Our hypothesis is that ME_{art} could be used to identify the suitable PCIS for the analyte by comparing the PCISs' ability for its correction. We demonstrate the utility of this approach in a proof-of-concept study, where 19 diverse SIL standards were spiked into plasma, urine, and feces. Their most suitable PCISs, selected based on compensation for biological ME (ME_{bio}) and ME_{art}, were then compared. Afterward, the efficiency of the ME_{art}-selected PCISs in correcting ME_{bio} was examined for the 19 SIL standards.

2. Material and method

2.1 Chemicals and materials

LC-MS-grade acetonitrile (ACN) and methanol (MeOH) were purchased from Actu-all chemicals (Randmeer, The Netherlands). Methyl tert-butyl ether (MTBE, ≥99.8%) was purchased from Sigma Aldrich (St. Louis, Missouri, United States). Formic acid (FA) was purchased from Biosolve B.V. (Valkenswaard, Netherlands), and hydrochloric acid (37% solution in water) was purchased from Acros organics (Geel, Belgium). Purified water was obtained from a Milli-Q PF Plus system (Merck Millipore, Burlington, Massachusetts, United States). Table S1 provides the supplier details of all standards, including the PCIS candidates, artificial matrix compounds and stable isotopically labeled (SIL) standards. EDTA plasma was obtained from Sanquin (Sanquin, Amsterdam, The Netherlands) and BioIVT (Westbury, NY, USA). Urine and fecal samples were collected from four healthy volunteers (age range: 23-35 years).

2.2 Solution preparation for PCISs, artificial matrix compounds and SIL standards.

Stock solutions of leucine-enkephalin (Leu-enk), fludrocortisone (F-Cor), 5-fluoroisatin (F-Isat), caffeine-$^{13}C_3$ (Caff-$^{13}C_3$), 3-fluoro-DL-valine (F-Val), D-glucose-d_7 (Glu-d_7) were prepared as described in Table S1. The stock solutions of all PCISs were diluted with 50% ACN in water to 50 µg/mL, 5 µg/mL, and 1 µg/mL for concentration optimization. L-homoarginine hydrochloride (hArgHC), sodium dodecyl sulphate (SDS), and tridodecylmethylammonium chloride (TDMAC) were dissolved in 50% ACN in water, while sodium acetate (NaOAc) was prepared in 20% ACN (Table S1). Those standards were used as artificial matrix compounds, and their stock solutions were diluted with 50% ACN in water for concentration optimization. The stock solution preparation of the 19 SIL standards and their concentrations after spiking in plasma, urine, and feces are described in Table S1 and Table S2, respectively.

2.3 Sample preparation

Fecal and plasma samples were prepared as previously reported.[28] Briefly, 20mg freeze-dried fecal samples were extracted by liquid-liquid extraction with the mixture of

water/MeOH/MTBE (v/v/v), then 90 µL of aqueous layer was dried and reconstituted in 50 µL water containing 0.1% FA. Plasma samples were prepared with protein precipitation: 100 µL of ice-cold MeOH was added to 25µL of plasma sample, followed by drying of the supernatant and reconstitution in 75 µL of water containing 0.1% FA. Urine samples were prepared identically to plasma samples. For ME evaluation for SIL standards, the mixture of SILs was spiked into biological and matrix-free samples after extraction.

2.4 LC-MS setup with post-column infusion

Sample measurements were performed using either a Shimadzu Nexera X2 LC system coupled to a TripleTOF 6600 mass spectrometer (SCIEX, Foster City, CA, USA) or a Waters Acquity UPLC Class II LC system coupled to TripleTOF 5600 mass spectrometry (SCIEX, Foster City, CA, USA). For both systems, an ESI source was used, and the same LC-MS conditions and the post column setup were applied, as detailed in our previous study.[28] In short, data were acquired under full scan mode over the *m/z* range of 60-800 Da in both positive and negative modes. The LC separation was achieved by using a Waters Acquity UPLC HSS T3 column (1.8 µm, 2.1 mm × 100 mm) over a 15 min gradient with 0.1% FA in water and 0.1% FA in ACN as mobile phases. The LC flow was diverted to waste at 7 min to decelerate contamination of the MS. A binary Agilent 1260 Infinity pump (Agilent Technologies, Santa Clara, USA) was used for post-column infusion at a flow rate of 20 µL min^{-1}. The post-column flow was combined with the LC eluent using a T connector (IDEX, PEEK Tee, 0.02 Thru hole, F-300) before injecting to the MS.

2.5 Data processing

Raw data were acquired by Analyst TF software 1.7.1 (SCIEX) and processed using SCIEX OS (version 2.1, SCIEX) and PeakView (version 2.2, SCIEX). Extracted ion chromatograms (EICs) for all PCIS candidates were obtained with an *m/z* window of 0.02 Da. A maximum mass error of 5 ppm was applied for peak integration of endogenous compounds and SIL standards. The infusion profiles of the PCIS candidates were generated by smoothing the extracted EIC data using the simple moving average

(SMA, n = 15) function in R (version 4.3.2). The ME profile (MEP) for each PCIS was generated as reported previously.[28]

Different types of ME were calculated for the SIL standards in plasma, urine, and feces, separately. The biological absolute matrix effect (AME_{bio_i}) and relative matrix effect (RME_{bio}) in each type of biological matrix (plasma, urine, feces) were calculated as shown in Equation 1 and 2. The calculation uses the integrated peak area (A) in a biological sample (*i*) from each biological matrix type (bio) (A_{bio_i}) and that in a matrix-free (solvent) sample (A_{sol}). The artificial absolute matrix effect (AME_{art_j}) created by artificial matrix was calculated as Equation 3. The artificial matrix includes individual artificial matrix compounds as well as their mixture, making different artificial matrix combinations (*j*). For each biological matrix, the integrated peak areas of the SIL standards in a pooled biological matrix type ($\overline{bio}$) with ($A_{art_j+\overline{bio}}$) and without ($A_{\overline{bio}}$) artificial matrix infusion were used for AME_{art_j}calculation. The relative artificial matrix effect (RME_{art}) was calculated as the relative standard deviation (RSD %) among the AME_{art_j} obtained from different artificial matrix combinations (Equation 4).

The PCIS-corrected response of each SIL was generated through integrating the ratio obtained from dividing the signal of a SIL standard by that of an individual PCIS at each time point with an in-house software. In each sample, the retention time and peak width of individual SIL standards before PCIS correction were used to identify the regions for ratio integration, and the integration of the PCIS-corrected signal was manually examined. The AME_{bio_i}, RME_{bio}, AME_{art_j}, and RME_{art} after PCIS correction were calculated as described in Equation 1-4, but with the replacement of peak area by PCIS-corrected area. To evaluate the overall ME caused by the biological matrix (ME_{bio}) or the artificial matrix (ME_{art}) for each matrix type, a scoring system combining the absolute matrix effect (AME) and relative matrix effect (RME) was applied, as shown in Table 1. For ME_{bio} score, the averaged AME_{bio_i} score from different individuals ($\overline{AME}_{bio_{1-i}}$) was used for the calculation, while the AME_{art} obtained from the artificial matrix compounds mixture ($AME_{art_{mix}}$) was used for ME_{art} scoring.

Equation 1: $\mathrm{AME}_{bio_i}(\%) = \frac{A_{bio_i}}{A_{sol}} * 100$

Equation 2: $\mathrm{RME}_{bio}(\%) = \frac{\mathrm{SD}(AME_{bio_1} \ldots AME_{bio_i})}{\mathrm{Mean}(AME_{bio_1} \ldots AME_{bio_i})} * 100$

Equation 3: $\mathrm{AME}_{art_j}(\%) = \frac{A_{art_j + \overline{bio}}}{A_{\overline{bio}}} * 100$

Equation 4: $\mathrm{RME}_{art}(\%) = \frac{\mathrm{SD}(AME_{art_1} \ldots AME_{art_j})}{\mathrm{Mean}(AME_{art_1} \ldots AME_{art_j})} * 100$

Table 1. The scoring system for absolute matrix effect (AME), relative matrix effect (RME), biological matrix effect (ME_{bio}), and artificial matrix effect (ME_{art})

Conditions*	**Scoring Formula**
AME <= 100	AME score = 100 * (AME/100)
AME > 100	AME score = 100 / (AME/100)
RME	RME score = 100 - RME
ME_{bio}	ME_{bio} score = ($\overline{AME}_{bio_{1-i}}$ score + RME_{bio} score) /2
ME_{art}	ME_{art} score = ($AME_{art_{mix}}$ score + RME_{art} score) /2

*AME (%) = 100 indicates no matrix effect; AME (%) < 100 indicates ion suppression; AME (%) >100 indicates ion enhancement

3. Results and discussion

3.1 PCIS method development

To develop a suitable PCIS approach for our untargeted metabolomics method, PCIS candidates with diverse structures were examined. Important factors such as adduct formation, infusion profile diversity, infusion concentration, room temperature stability, and matrix effect profile (MEP) diversity were evaluated. Plasma, urine, and feces were used in the selection process, ensuring selected PCIS could be effectively applied across diverse biological matrices.

3.1.1 PCIS selection and infusion concentration optimization

Ideally, a PCIS should be commercially affordable, measurable with specific signal, detectable mainly with protonated $[M+H]^+$ and deprotonated $[M-H]^-$ ions, and stable during analysis.[29] With this in mind, six xenobiotic compounds with different physicochemical properties were evaluated as PCIS candidates in our study. All six standards were examined in positive ionization mode, and five were assessed in negative ionization mode. (Table S3). First, we examined the adduct formation of all the PCIS candidates: $[M+H]^+$ and $[M-H]^-$ were the ions with highest response for most of the candidates, except for Glu-d_7 in positive mode and F-cor in negative mode. The former showed a higher signal with sodium ($[M+Na]^+$) and ammonium ($[M+NH_4]^+$) adducts than with $[M+H]^+$, while the latter had a higher signal as the formic acid adduct ($[M+FA-H]^-$) compared to $[M-H]^-$. In addition to $[M-H]^-$, Glu-d_7 also showed good intensity with $[M+FA-H]^-$. Considering that the infusion profiles of a PCIS may vary with different adducts,[30] for Glu-d_7, we monitored both $[M+Na]^+$ and $[M+NH_4]^+$ in positive mode, as well as both $[M-H]^-$ and $[M+FA-H]^-$ in negative mode. However, only $[M+FA-H]^-$ was monitored for F-Cor in negative mode, as the signal of $[M-H]^-$ was too low to generate a stable infusion profile.

Subsequently, Pearson correlation was applied to evaluate the diversity of the infusion profiles among PCIS candidates. The EICs of all PCIS candidates were extracted and correlated with each other after the injection of plasma samples. This procedure was repeated with four different plasma samples to include sample diversity. As shown in Table S4-5, Leu-enk showed a near identical infusion profile to F-Val in positive mode ($r > 0.95$ in three examined plasma samples), and to F-Isat in negative mode ($r > 0.99$ in all examined plasma samples). Therefore, five PCIS (Leu-enk, F-Cor, F-Isat, Caff-$^{13}C_3$, Glu-d_7) were selected for positive mode, and four (Leu-enk, F-Cor, F-Val, Glu-d_7) for negative mode.

Table 2. Monitored ions and optimized infusion concentrations for selected PCISs

PCIS		Detected ions		Infusion concentration (ng/mL)	
full name	abbreviation	positive	negative	positive	negative
Leucine-enkephalin	Leu-enk	$[M+H]^+$	$[M-H]^-$	212.4	344.9
Fludrocortisone	F-Cor	$[M+H]^+$	$[M+FA-H]^-$	154.0	371.0
D-glucose-d_7	Glu-d_7	$[M+Na]^+$, $[M+NH_4]^+$	$[M-H]^-$, $[M+FA-H]^-$	5734.0	6465.7
5-Fluoroisatin	F-Isat	$[M+H]^+$	/	1069.2	/
Caffeine-$^{13}C3$	Caff-$^{13}C_3$	$[M+H]^+$	/	219.2	/
3-Fluoro-DL-valine	F-Val	/	$[M-H]^-$	/	4264.3

After selection, the infused concentrations of the PCISs were optimized to balance the trade-off between signal intensity and PCIS-induced ME. Concentration optimization is widely discussed in studies applying PCIS,[12,17,22,29] and the ubiquitous goal is to achieve stable infusion signal without inducing additional ME. Figure 1A presents infusion profiles of the PCISs extracted from one plasma sample at the optimized PCIS infusion concentrations (Table 2). In both ionization modes, the initial intensities of the main monitored ions were above 20,000 cps for all PCISs, which was high enough for clear and stable signal monitoring. Stable infusion signals were monitored for all PCISs over plasma injections (Figure S1A-B). Although there were regions (0.5-0.8 min, 1.5-1.8 min) with severe signal suppression, the lowest signals of the PCISs remained above 100 cps. The exceptions were $[Glu\text{-}d_7+NH_4]^+$ in positive mode, and $[Glu\text{-}d_7+FA\text{-}H]^-$ in negative mode at 0.5-0.8 min, as shown in the zoomed-in sections at the top left of Figure 1A.

To assess whether the selected PCISs were also applicable in other biological matrices at the optimized concentrations, the infusion profiles of the PCISs were inspected in three different urine (Figure S1C-D) and fecal samples (Figure S1E-F). The infusion profiles of each PCIS were constructed in urine and feces by averaging signals from three individuals, as presented in Figure 1B and 1C. Similar to plasma, the initial infusion signals were above 20,000 cps and the lowest infusion signals of the PCISs were above 100 cps in both urine and fecal samples. This indicated that abundant and

stable infusion profiles were also achieved for the selected PCISs at the optimized concentrations in plasma and feces.

Then, we evaluated the impact of PCISs on analyte signals by comparing the peak areas of several known metabolites in the same plasma sample, with and without PCIS infusion. In total, 60 targets were used for the signal comparison in positive mode, and 36 in negative mode (Table S6). As shown in Figure 1D, no significant differences in peak areas were found for the examined metabolites with and without PCIS infusion in both ionization modes. Compared with infusion, the signal changes of most examined metabolites with PCIS are within ±30% (Table S6). Additionally, the room temperature stability of the selected PCIS was examined over seven days by injecting the PCIS mixture solution in positive mode. From day 1 to day 7, the signal variations of all PCISs were within 10% compared to the freshly prepared solution on day 0. (Figure S2).

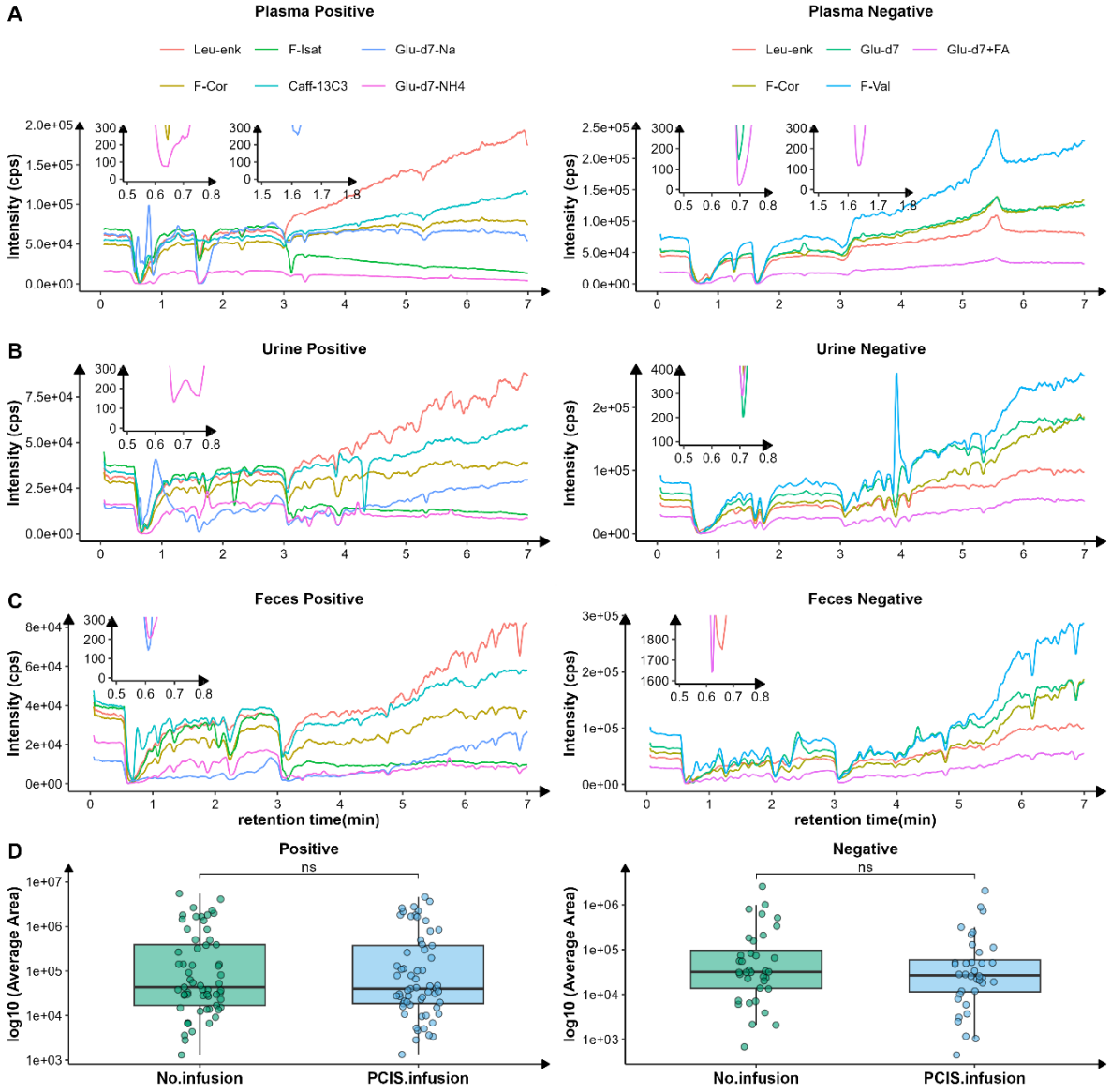

Figure 1. Infusion profiles over 0-7 mins and zoomed-in inspections of regions with severe suppression for the selected PCISs in plasma (A), urine (B) and feces (C), as well as the peak area comparison between plasma injections with and without PCIS infusion in positive and negative ionization modes (D). The intensities plotted in (A) and the peak area for each examined metabolites used in (D) were the mean values from duplicated injections of the same plasma sample; the intensities plotted in (B) and (C) are the mean values of three different individuals; A two-side unpaired t test was applied for statistical assessment in (D).

3.1.2 PCIS diversity evaluation with matrix effect profiles

To clearly identify ion suppression and enhancement over the entire chromatography, the infusion profiles of the PCISs in each biological matrix were normalized against those in the solvent samples, creating the MEP.[19] The MEPs of each PCIS, generated with three different individuals from plasma, urine, and feces, are presented in Figure S3. The averaged MEP for each PCIS ($\overline{\text{MEP}}$) was calculated from the MEPs of different individuals in each biological matrix, and the $\overline{\text{MEP}}$ variation plots were created by overlaying the $\overline{\text{MEP}}$ of all PCISs. As shown in Figure 2A, for each matrix and ionization mode, the solid line represents the overall AME monitored with all PCISs, while the shaded area shows the variations of the $\overline{\text{MEP}}$ among all PCISs.

To directly display the $\overline{\text{MEP}}$ variation among the PCISs, the RSD% of the $\overline{\text{MEP}}$ was calculated per timepoint and plotted for each biological matrix, as presented in Figure 2B. The RSD% of the $\overline{\text{MEP}}$ monitored with the same set of PCISs varied among plasma, urine and feces. In plasma, high diversity was mainly observed in the early elution region (RT < 2 min), with RSD > 15% in both ionization modes. In urine, apart from the early elution regions, diverse MEPs were also noted within 2-4 mins, particularly in positive mode. In feces, the RSD % of the $\overline{\text{MEP}}$ was above or close to 15 % almost throughout the entire chromatogram in both ionization modes. Considering the matrix complexity, it is expected that the $\overline{\text{MEP}}$ variation is larger in feces than in urine and plasma. This observation is consistent with the study by Stahnke *et al*., who reported that a more complex matrix can induce larger variations among infused pesticides.[19] Tisler *et al.* also observed that, compared to diluted waste water, the waste water with more concentrated matrix varied more in MEP compared to the diluted one.[31] In our study, the diversity of the three biological matrices is successfully reflected by the $\overline{\text{MEP}}$ variation of selected PCISs, making it feasible to apply these PCISs to assess the ME from less to more complex biological matrices.

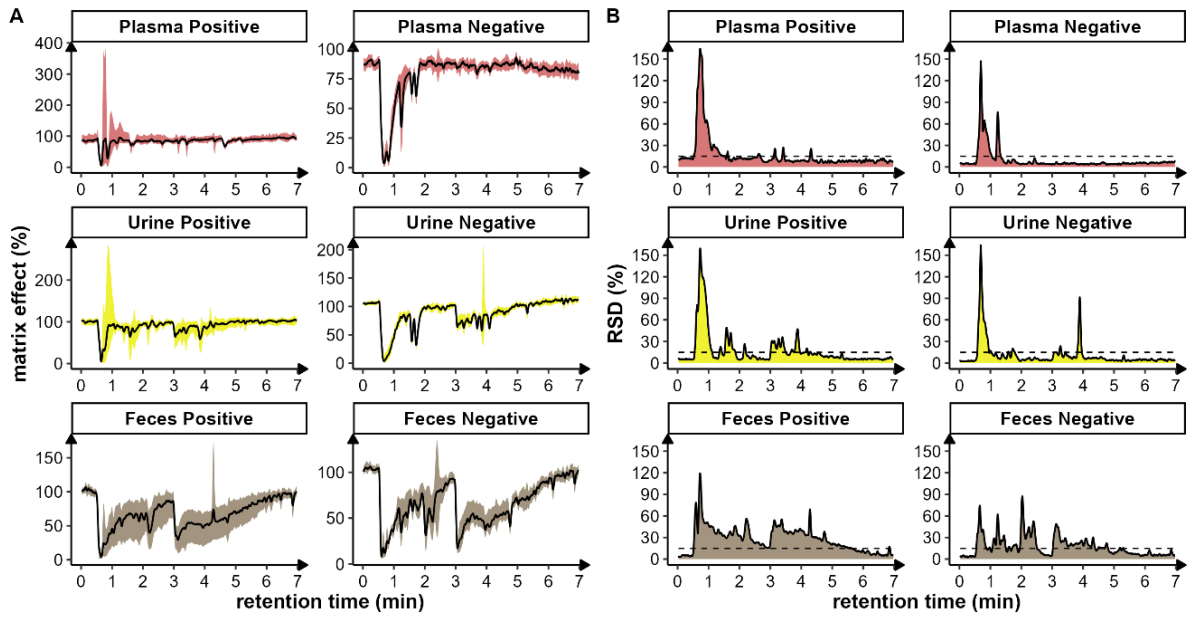

Figure 2. MEP variation plots with overlaid averaged MEP ($\overline{MEP}$) among all the PCIS (A) and RSD of the $\overline{MEP}$ (B) for all PCISs in plasma, urine, and feces for both ionization modes. The dashed line in (B) indicates where RSD is 15%.

3.2 PCIS matching using post-column artificial matrix effect creation

With multiple PCISs available, it's crucial to select one that resembles the analyte in its susceptibility to ion suppression or enhancement to effectively correct for its ME. Therefore, we introduced an approach, post-column artificial ME creation, to the developed LC-PCIS-MS method to match analytes to their suitable PCISs. In this approach, along with the PCIS, the artificial matrix, consisting of a set of compounds that create ME, was continuously infused to the ESI source after the LC column, inducing the ME_{art}. The ME_{art} for a given analyte can be determined by comparing its response with and without artificial matrix infusion. Then, the best-match PCIS for that feature can be selected based on its ability to compensate for the observed ME_{art}. Our hypothesis is that the best-match PCIS selected based on ME_{art} correction should also be effective in compensating for ME_{bio}. This hypothesis depends greatly on how well the infused artificial matrix can mimic the biological matrix to induce ME in the ESI source. Therefore, we selected several compounds according to known ME mechanisms in the ESI source and optimized their concentrations to induce certain ME_{art} for the metabolites examined. This hypothesis was evaluated by comparing the best-match

PCISs selected based on ME_{art} correction with those chosen for ME_{bio} compensation using 19 SIL standards (Table S2).

3.2.1 Selection and concentration optimization of post-column infused artificial matrix compounds

In the ESI source, matrix compounds can disturb the ionization by competing with the analytes for charge in liquid phase and affecting the analytes' ability to remain charged in gas phase.[2] Considering this, four compounds, l-homoarginine hydrochloride (hArgHC), sodium dodecyl sulphate (SDS), sodium acetate (NaOAc), and tridodecylmethylammonium chloride (TDMAC), were chosen as artificial matrix compounds to interrupt the ionization process in the ESI source. These compounds contain salts and/or ionic compounds which can easily form charged ions, competing with analytes for ionization. Additionally, hArg has a high proton affinity in gas-phase;[32] SDS and TDMAC can prevent the coulombic explosion by increasing the droplet's surface tension as surfactants.[33] Based on their ionization properties, hArgHC, NaOAc, and TDMAC were infused in positive mode, while SDS and NaOAc in negative mode.

The concentrations of the artificial matrix compounds were optimized by infusing them individually as well as in a mixture with the injection of pooled plasma, urine and fecal samples. This allowed us to calculate both AME_{art} and RME_{art} with a pooled biological sample, as shown in Equation 3-4. To balance the trade-off between ME_{art} and signal intensity of endogenous metabolites, the optimization aimed to get around 70% AME_{art} and more than 15% RME_{art}. During the optimization process, 19 and 24 endogenous metabolites were evaluated in positive and negative ionization modes, respectively. The average AME_{art} of all the evaluated metabolites at the optimized concentrations (Table 3) are plotted in Figure 3A-B, while the individual AME_{art} are shown in Figure S4. Compared to infusion without artificial matrix (PCIS only), infusing the mixtures successfully induced AME_{art} to 60-70% in plasma, urine and feces for both ionization modes. For individual artificial matrix compounds, hArgHC and SDS at 1µM barely caused signal suppression in positive and negative modes, respectively; NaOAc showed a pronounced ion suppression effect, bringing AME_{art} to 70-75% for both ionization

modes, except for urine in negative mode; TDMAC suppressed the signal of the examined metabolites in plasma and urine, resulting in around 75% AME_{art} in positive mode. Given that diverse ion suppression effects were observed with different artificial matrix combinations, RME_{art} was calculated with all combinations for each ionization mode. As illustrated in Figure 3C-D, the RME_{art} of most metabolites were above 15 % in both ionization modes for all three biological matrices, with several of them exceeding 30%.

Meanwhile, with artificial matrix infusion, the PCISs should experience similar signal suppression to ensure their ability to correct ME_{art}, hence, their infusion profiles were inspected to determine whether their signals were correspondingly suppressed. The PCIS profiles in feces, with and without the mixture, are presented in Figure S5-6 as examples. The artificial matrix successfully suppressed the signal of all PCISs in positive mode, except for $[Glu\text{-}d_7 + Na]^+$. Its signal was largely enhanced by the artificial matrix infusion, which was likely due to the high sodium content in NaOAc (Figure S5A). This resulted in a much lower signal for $[Glu\text{-}d7 + NH_4]^+$, especially in regions with severe ion suppression (Figure S5B). Due to the distorted adduct distributions caused by artificial matrix, $Glu\text{-}d_7$ was not considered as a suitable PCIS for ME correction in positive mode in our study. In negative mode, the artificial matrix also suppressed the signal of all PCISs, except for $[F\text{-}Cor+FA\text{-}H]^-$ and $[Glu\text{-}d7 +FA\text{-}H]^-$, which had comparable intensity with and without artificial matrix infusion over 1-5 mins (Figure S6). These results proved that, at the optimized concentration, infusing the mixture of artificial matrix compounds could successfully induce ion suppression for both metabolites and PCISs.

Table 3. Information and optimized infusion concentrations of artificial matrix compounds

Artificial matrix compound		**Infusion concentration (µM)**	
full name	abbreviation	positive	negative
L-homoarginine hydrochloride	hArgHC	1.0	/
sodium dodecyl sulphate	SDS	/	1.0

sodium acetate	NaOAc	500	375.0
tridodecylmethylammonium chloride	TDMAC	37.5	/

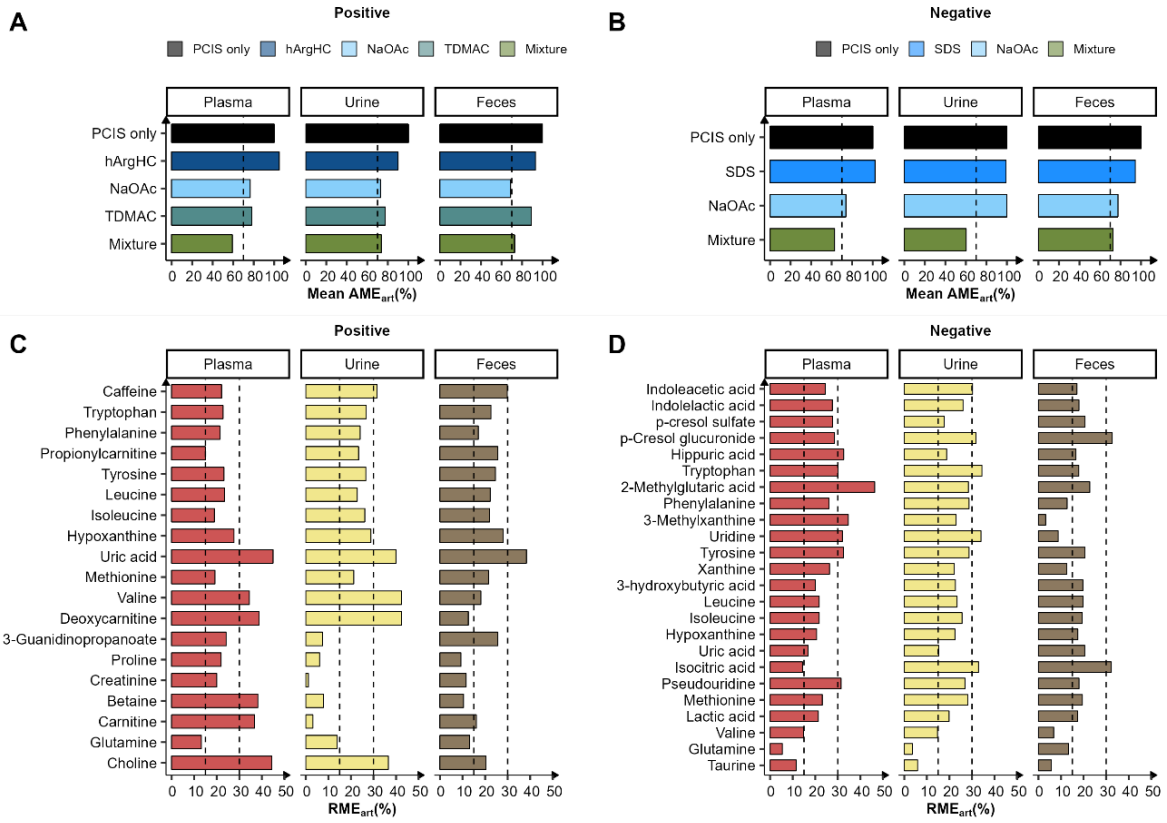

Figure 3. The artificial matrix induced AME_{art} (A, B) and RME_{art} (C, D) for metabolites examined in plasma, urine, and feces. The mean AME_{art} was calculated by averaging the AME_{art} for the examined metabolites in each ionization mode with duplicates, and PCIS only was used as reference with AME_{art} = 100%. The dashed lines in (A) and (B) indicate 70% AME_{art}. The RME_{art} for each metabolite is presented as the RSD % of the AME_{art} among all infusion combinations in positive (C) and negative (D) modes, including PCIS only. The dashed lines in (C) and (D) indicate 15% and 30 % RME_{art}.

3.2.2 PCIS matching: ME_{art} correction vs. ME_{bio} correction

With the optimized artificial matrix concentration, we compared the best-match PCISs selected based on their ability to correct the ME_{art} or the ME_{bio} for 19 SIL standards. These standards were widely distributed in class and physical properties, representing

diverse endogenous metabolites. The AME and RME of the SIL standards were calculated after being spiked into plasma, urine, and fecal samples, as described in 2.5.

To combine both AME and RME for PCIS selection, they were scored as described in Table 1. The final ME scores were calculated by average the AME and RME scores. AME_{bio} and RME_{bio} were calculated at two concentration levels (Table S2), and the averaged areas of two levels were used for ME_{bio} scoring. AME_{art} and RME_{art} were calculated at one concentration level (Table S2). An AME within 80-120% and a RME ≤ 30% are commonly accepted in untargeted analysis,[34] which results in an AME score ≥ 80 and a RME score ≥ 70. Therefore, a PCIS is considered suitable for correcting ME_{bio} or ME_{art} for a SIL standard if it returns a ME score ≥ 75 after correction.

Figure S7 shows the ME_{bio} and ME_{art} scores for 19 SIL standards spiked in plasma, urine, and feces before and after PCIS correction. To identify the suitable PCISs for ME correction, the PCISs were filtered with an ME score ≥ 75. Figure 4 presents the ME scores before and after correction with the filtered PCISs. Before PCIS correction, early-eluting (retention time < 1 min) SIL standards (L-ornithine-d_6, L-glutamine-d_5, TMAO-d_9, L-carnitine-d_3, N-methy-d_3-L-histidine, and betaine-d_9) in three biological matrices, hippuric acid-d_5 in urine, and daidzein-d_6 in feces suffered from more severe ME_{bio}, with scores < 75 (Figure 4A). In contrast to ME_{bio}, most of the early eluting SIL standards had ME_{art} above 75, while more later eluters got ME_{art} scores < 75 before PCIS correction (Figure 4B). It is likely that with artificial matrix infusion, the biological matrix remained as the major source of ionization competition in the early elution region, where the ME_{art} was masked by severe ME_{bio}. Some known endogenous ion suppressors, such as inorganic electrolytes, salts, and highly polar compounds, are poorly retained on the RP column, leading to pronounced ion suppression that overwhelms the influence of artificial matrix in the early elution region. This was reversed in the late elution regions where the artificial matrix had a greater impact on ionization than the biological matrix. The filtered PCISs improved or maintained the ME scores for the SIL standards with initial scores ≥ 75 and successfully compensated for the ME for most of the SIL standards with ME_{bio} or ME_{art} scores ≤ 75 before PCIS correction (Figure 4). For those SIL standards had no PCISs to improve their ME scores

to 75, mainly for the ME_{bio} correction of early-eluting ones in urine and feces, most of them still obtained improved scores after PCIS correction (Figure S7A).

Considering that more than one PCISs managed to correct either ME_{bio} or ME_{art} for most SIL standards (Figure 4), to obtain an overview of which PCIS was appropriate for compensating ME regardless of matrix types, we summed the ME_{bio} or ME_{art} scores of the filtered PCISs for individual SIL standards across plasma, urine, and feces. With 75 as the acceptable ME score, a PCIS score sum between 75 and 100 indicated its capability to correct ME in one biological matrix; between 150 and 225 indicated effective correction in two biological matrices; a score sum above 225 indicated correction in all three biological matrices. Then, the matrix-independent PCIS can be identified by selecting the one with the highest score sum for each SIL standard.

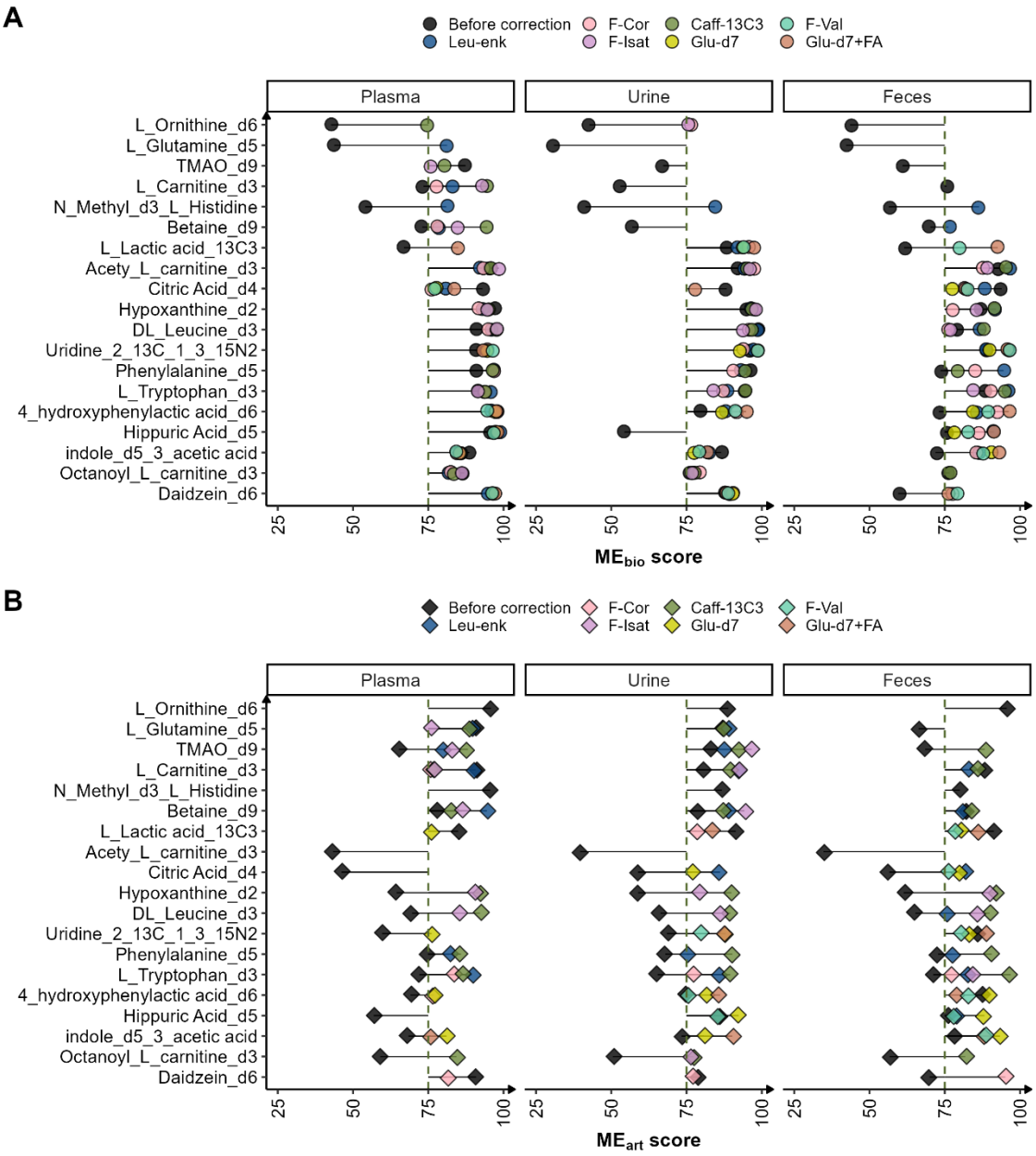

Figure 4. ME_{bio} (A) and ME_{art} (B) scores of the SIL standards before correction (dots and diamonds in black) and after correction with suitable PCISs (dots and diamonds with colors) in plasma, urine, and feces. The SIL standards are plotted in increasing order of retention times from top to bottom and the dashed lines indicate a score of 75, and triplicates were used for ME_{bio} score and ME_{art} score calculation.

The score sums of the filtered PCISs for the SIL standards are presented in Figure 5A. In total, 13 and 12 out of 19 SIL standards had at least one PCIS with an ME_{bio} score sum and ME_{art} score sum ≥ 225, respectively. More PCISs returned an ME_{art} score sum

≥ 150 compared to ME_{bio} score sum for the early-eluting SIL standards. In contrast, for the SIL standards eluting after one minute, all the filtered PCISs returned ME_{bio} score sums ≥ 150, except for lactic acid-$^{13}C_3$. More PCISs achieved an ME_{bio} score sum ≥ 225 for those SIL standards compared to ME_{art} score sum. Given that the early-eluting SIL standards experienced more ME_{bio} than ME_{art}, while the later-eluting ones were more affected by ME_{art} than ME_{bio} (Figure 4), these results suggest that correcting a severe ME is likely to facilitate the selection of the matrix-independent PCIS for a SIL standard. This is also evidenced by comparing the filtered PCIS for ME_{bio} correction in plasma, urine, and feces (Figure 4A). For instance, lactic acid-$^{13}C_3$ experienced more ME_{bio} in plasma and feces. Compared to five PCIS suitable for ME_{bio} correction in urine, only one and two were suitable for the correction in plasma and feces, respectively. Similarly, hippuric acid-d_5 experienced severe ME_{bio} only in urine, with no PCIS suitable for correction, whereas multiple PCISs corrected its ME_{bio} in plasma and feces. Additionally, since daidzein-d_6 had an ME_{bio} score < 75 only in feces before correction, three PCISs were ideal for correcting its ME_{bio} in feces, while all PCISs were suitable for the correction in urine and plasma.

Therefore, we assumed that for the SIL standards experiencing more severe ME_{art} than ME_{bio}, the PCIS selected based on ME_{art} compensation would also be effective in correcting their ME_{bio}. To evaluate this assumption, we compared the best-match PCIS identified by the highest ME_{bio} score sum to those selected by the highest ME_{art} score sum. Three SIL standards (L-ornithine-d_6, N-methyl-d_3-L-histidine, acety-L-carnitine-d_3) did not have a suitable PCIS with an ME_{art} score ≥ 75 in any of the examined biological matrices. Their ME_{art}-based best-match PCISs were still selected based on the highest ME_{art} score sum to include them in the comparison. Figure 5B presents the selected best-match PCISs for all SIL standards according to the highest ME_{bio} score sum or the highest ME_{art} score sum. Ten SIL standards (connected by solid line) obtained identical best-match PCISs based on the selection of ME_{bio} and ME_{art} score sums. Seven standards (connected by dashed line) had different best-match PCISs. However, their PCISs selected based on the highest ME_{art} score sums returned comparable ME_{bio} score sums to those chosen with the highest ME_{bio} score sum, making them equally suitable for ME_{bio} correction. Two standards (unconnected), L-ornithine-

d6 and citric acid-d4, exhibited different best-match PCISs. Consequently, 17 out of 19 SIL standards (89%) showed consistency in PCIS selection based on ME_{bio} and ME_{art} score sums, including some SIL standards experiencing severe ME_{bio} than ME_{art}, such as most of the early eluters and L-lactic acid-$^{13}C_3$. This suggests that, although ME_{art} may be less effective in identifying the matrix-independent PCISs for the SIL standards experiencing a more severe ME_{bio} than ME_{art}, utilizing the ME_{art} score sum across diverse matrices may enhance the likelihood of making suitable selections.

These results demonstrate that ME_{art} compensation obtained comparable PCIS selections to the ME_{bio} correction for the examined SIL standards across diverse matrices. The ME_{bio} correction, namely matching PCISs to analytes by assessing their ability to correct for ME quantified with spiked SIL standards, has been commonly applied in targeted metabolomics studies[13,14,23] However, this approach is impractical for untargeted metabolomics due to the reliance on SIL standards. Another strategy for PCIS selection is to evaluate the improvement in linearity and precision across matrix dilution series before and after PCIS correction.[15,18,29] Although this method is applicable for untargeted analysis as it does not require authentic standards spiking, it can be problematic for metabolites with rather high or low endogenous abundance due to potential solubility and detection limit issues.[29] Therefore, the reliability of ME_{art} compensation in PCIS selection is supported not only by its consistency with the ME_{bio} correction, but also by mitigating the risk of the analyte signals falling beyond their limits of detection/quantification. More importantly, since the ME_{art} can be determined for any detected feature, the ME_{art} compensation represents an ideal approach for PCIS matching in untargeted metabolomics.

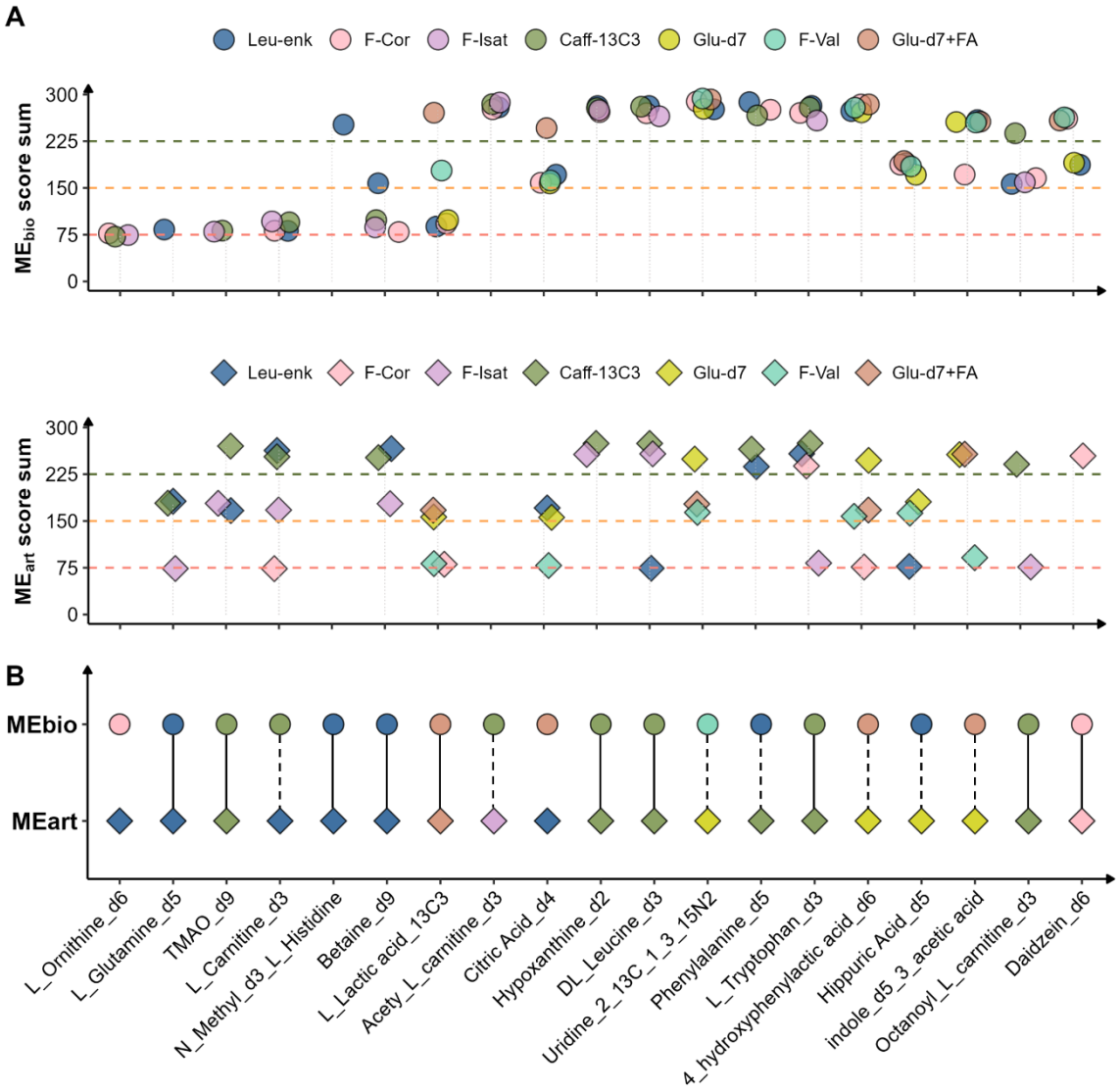

Figure 5. The ME_{bio} and ME_{art} score sum of all the SIL standards across plasma, urine, and feces for the PCISs that returned scores ≥ 75 in at least one biological matrix (A). The selected PCISs according to the highest ME_{bio} and ME_{art} score sums across plasma, urine, and feces for the SIL standards (B), where the solid line connection indicates identical PCIS selection, while the dashed line connection indicates PCIS selection with comparable score sums, and no connection indicates different PCIS selection. The SIL standards are plotted in increasing order of retention times from left to right.

3.3 ME_{bio} correction with PCIS selected by ME_{art}

To assess the effectiveness of ME_{art}-selected PCIS in ME_{bio} correction, we applied the PCIS selected with the highest ME_{art} score sum for ME_{bio} correction of the 19 SIL

standards spiked in plasma, urine, and feces. The ME_{bio} scores of all the SIL standards before and after PCIS correction is plotted in Figure S8. The selected PCIS improved or maintained the ME_{bio} score for 19 (100%), 16 (84%), and 18 (95%) SIL standards spiked in plasma, urine, and feces, respectively.

To illustrate the improvement in ME after PCIS correction, the AME_{bio} and RME_{bio} values of the 19 SIL standards were compared before and after correction in each biological matrix. As presented in Figure 6, the dots represent the AME_{bio} value (left y axis), whereas the bars indicate the RME_{bio} value (right y axis). In plasma (Figure 6A), seven SIL standards, namely the six early eluters and lactic acid-$^{13}C_3$, experienced ion suppression with AME_{bio} < 80% before correction. The PCIS improved the AME_{bio} towards 80 -120% for five of them, bringing the AME_{bio} of N-methyl-d_3-L-histidine and lactic acid-$^{13}C_3$ within the acceptable range. The RME_{bio} of all SIL standards were below 30% after PCIS correction, with significant improvements for L-ornithine-d_6, L-glutamine-d_5, and lactic acid-$^{13}C_3$. In urine (Figure 6B), nine SIL standards, including the early eluters, 4-hydroxyphenylactic acid-d_6, hippuric acid-d_5, and octanoyl-L-carnitine-d_3, had AME_{bio} outside 80 -120%. After PCIS correction, five standards showed improved AME_{bio}, with N-methyl-d_3-L-histindine and 4-hydroxyphenylactic acid-d_6 reaching the range of 80-120%. The RME_{bio} of all SIL standards were within 30% after PCIS correction in urine, except for hippuric acid-d_5. Significant improvements were noted for L-glutamine-d_5, L-carnitine-d_3, and betanine-d_3, which had RME_{bio} greater than 30% before correction. In feces (Figure 6C), 13 SIL standards suffered from ion suppression (AME_{bio} < 80%) or enhancement (AME_{bio} > 120%) before PCIS correction. After correction, 10 of them showed improved AME_{bio} approaching the 80-120% range, with five within the range. Four SIL standards exhibited RME_{bio} close to or exceeding 30% before correction; the PCIS successfully reduced the RME_{bio} of lactic acid-$^{13}C_3$ and daidzein-d_6 to below 15%.

Over-corrected AME_{bio} or increased RME_{bio} were observed for TMAO-d_9, L-carnitine-d_3, and betaine-d_9, in all biological matrices. This seems to be caused by the permanent positive charge at the quaternary ammonium group in these early eluters, which makes them less susceptible to ion suppression than the PCISs in the region with severe

suppression. Considering that their PCIS selections were consistent based on the ME_{bio} and ME_{art} score sums (Figure 5B), another PCIS candidate with permanent charge may need to be included for ME correction of those standards. In addition, the selected PCIS failed to maintain or improve the AME_{bio} or/and RME_{bio} for citric acid-d_4, hippuric acid-d_5, and indole-d_5-acetic acid in urine. These SIL standards showed maintained or improved ME in the other two biological matrices, except for citric acid-d_4 in plasma. This inefficient correction is likely due to specific co-eluting matrix compounds present in urine, suggesting that a more acidic PCIS may be needed to mimic the ionization of those SIL standards for effective ME correction in urine. Overall, compared with no correction, PCISs selected by ME_{art} improved the ME_{bio} for most SILs affected by ME in the examined matrices, and maintained the ME_{bio} for those with acceptable ME prior to correction, demonstrating the reliability of ME_{art}-selected PCIS for ME_{bio} compensation.

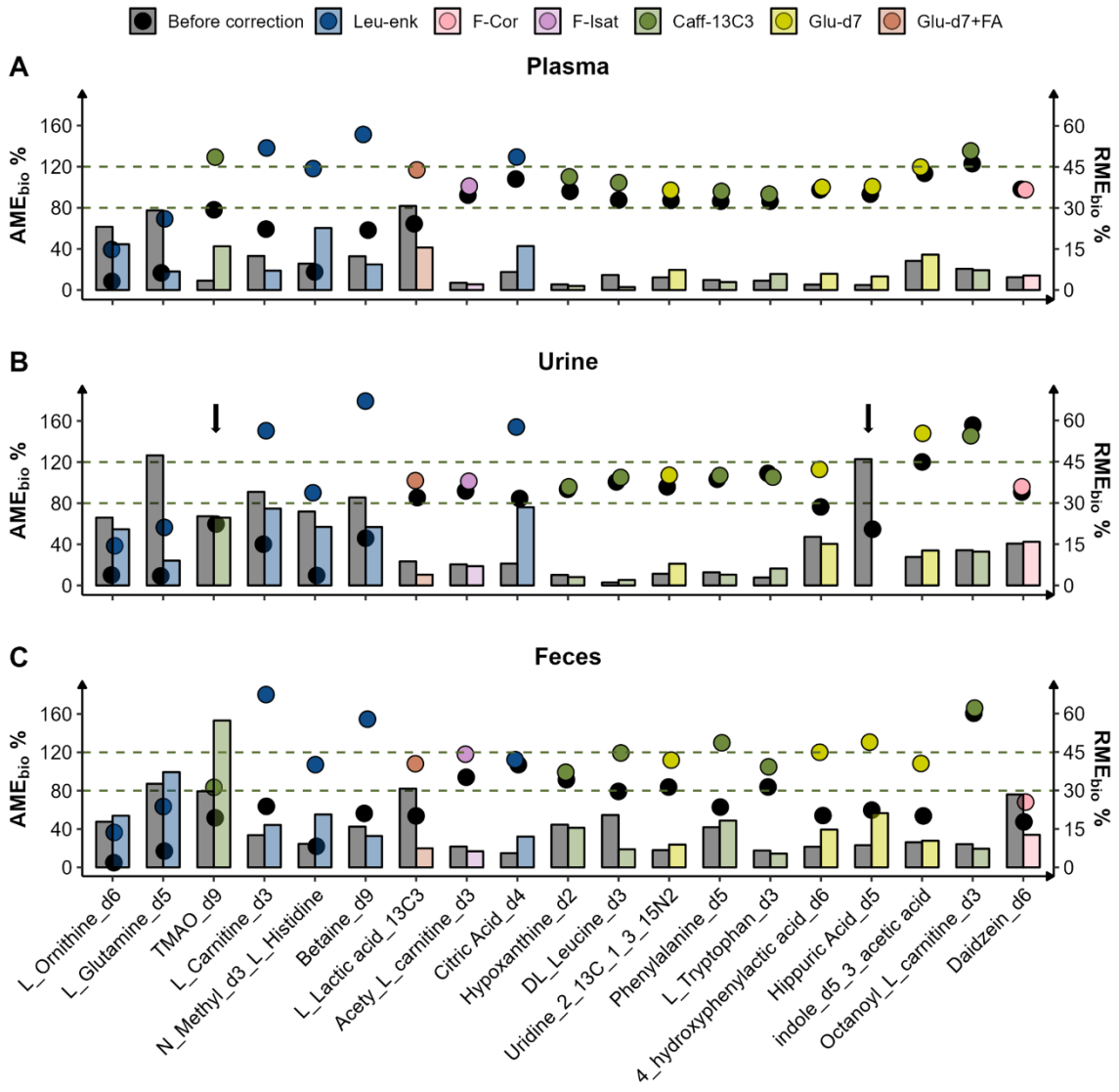

Figure 6. AME_{bio} (dots, left y axis) and RME_{bio} (bars, right y axis) of the 19 SIL standards spiked in plasma, urine, and feces before and after correction with the PCISs selected by the highest ME_{art} score sum. The SIL standards are plotted in increasing order of retention time from left to right. The dashed lines indicated 80-120% of AME_{bio}. The black arrows in (B) indicate the AME_{bio} higher than 160% and/or RME_{bio} larger than 60%.

4. Conclusion

In this study, we presented a strategy in an LC-PCIS-MS method for selecting suitable PCISs to compensate for ME in untargeted metabolomics. This is achieved by comparing the PCISs' ability to correct for the ME_{art} created through post-column

infusion of compounds that affect the ionization in the ESI source. A ME score system was introduced to incorporate AME and RME into the selection. To give equal importance to AME and RME, their average score was used as the final ME score in our study. Different weights can be assigned to AME and RME if one is considered more important than the other in a particular study.

The feasibility of ME_{art} compensation in identifying suitable PCIS was evaluated using 19 SIL standards spiked in plasma, urine, and feces. This evaluation was conducted by comparing the PCISs selected based on the ME_{art} and ME_{bio} compensation across the three matrices. As a result, 89% of the SIL standards showed consistent PCIS selection between ME_{bio} and ME_{art}, demonstrating the effectiveness of ME_{art} compensation for PCIS selection. Subsequently, we applied the ME_{art}-selected PCISs to correct for the ME_{bio} for the SIL standards, resulting in improved ME_{bio} for most of the SIL standards experiencing ME and maintaining ME_{bio} for those with acceptable ME before correction.

In conclusion, we demonstrate the concept of applying ME_{art} creation and compensation for PCIS matching in an LC-PCIS-MS method to correct for ME across diverse biological matrices. Importantly, this strategy is independent of retention time and standards spiking, making it universally applicable for any detectable feature in untargeted metabolomics. Ideally, based on the ME_{art} -selected PCISs, a feature-PCIS-matched library could be developed. Depending on the purpose of the study, such a library could be constructed with diverse or specific matrices and applied for ME correction in future studies. Overall, our study has proposed a novel approach to compensate for the ME in untargeted metabolomics with PCIS, which contributes to improving data reliability and comparability for untargeted metabolomic studies across varied matrices.

Acknowledgements

Pingping Zhu Would like to acknowledge the China Scholarship Council (CSC, No. 201906240049). This research was part of the Netherlands X-omics Initiative and partially founded by NWO project 184.034.019. This publication is part of the 'Building the infrastructure for Exposome research: Exposome-Scan' project (with project number 175.2019.032) of the program ‘Investment Grant NWO Large', which is funded by the Dutch Research Council (NWO).

Reference:

(1) González, O.; Blanco, M. E.; Iriarte, G.; Bartolomé, L.; Maguregui, M. I.; Alonso, R. M. Bioanalytical Chromatographic Method Validation According to Current Regulations, with a Special Focus on the Non-Well Defined Parameters Limit of Quantification, Robustness and Matrix Effect. *Journal of Chromatography A* **2014**, *1353*, 10–27. https://doi.org/10.1016/j.chroma.2014.03.077.

(2) Panuwet, P.; Hunter Jr., R. E.; D’Souza, P. E.; Chen, X.; Radford, S. A.; Cohen, J. R.; Marder, M. E.; Kartavenka, K.; Ryan, P. B.; Barr, D. B. Biological Matrix Effects in Quantitative Tandem Mass Spectrometry-Based Analytical Methods: Advancing Biomonitoring. *Critical Reviews in Analytical Chemistry* **2016**, *46* (2), 93–105. https://doi.org/10.1080/10408347.2014.980775.

(3) Matuszewski, B. K.; Constanzer, M. L.; Chavez-Eng, C. M. Strategies for the Assessment of Matrix Effect in Quantitative Bioanalytical Methods Based on HPLC−MS/MS. *Anal. Chem.* **2003**, *75* (13), 3019–3030. https://doi.org/10.1021/ac020361s.

(4) Cortese, M.; Gigliobianco, M. R.; Magnoni, F.; Censi, R.; Di Martino, P. Compensate for or Minimize Matrix Effects? Strategies for Overcoming Matrix Effects in Liquid Chromatography-Mass Spectrometry Technique: A Tutorial Review. *Molecules* **2020**, *25* (13), 3047. https://doi.org/10.3390/molecules25133047.

(5) Thakare, R.; Chhonker, Y. S.; Gautam, N.; Alamoudi, J. A.; Alnouti, Y. Quantitative Analysis of Endogenous Compounds. *Journal of Pharmaceutical and Biomedical Analysis* **2016**, *128*, 426–437. https://doi.org/10.1016/j.jpba.2016.06.017.

(6) Wang, S.; Cyronak, M.; Yang, E. Does a Stable Isotopically Labeled Internal Standard Always Correct Analyte Response?: A Matrix Effect Study on a LC/MS/MS Method for the Determination of Carvedilol Enantiomers in Human Plasma. *Journal of Pharmaceutical and Biomedical Analysis* **2007**, *43* (2), 701–707. https://doi.org/10.1016/j.jpba.2006.08.010.

(7) Berg, T.; Strand, D. H. 13C Labelled Internal Standards—A Solution to Minimize Ion Suppression Effects in Liquid Chromatography–Tandem Mass Spectrometry Analyses of Drugs in Biological Samples? *Journal of Chromatography A* **2011**, *1218* (52), 9366–9374. https://doi.org/10.1016/j.chroma.2011.10.081.

(8) Bonfiglio, R.; King, R. C.; Olah, T. V.; Merkle, K. The Effects of Sample Preparation Methods on the Variability of the Electrospray Ionization Response for Model Drug Compounds. *Rapid Communications in Mass Spectrometry* **1999**, *13* (12), 1175–1185. https://doi.org/10.1002/(SICI)1097-0231(19990630)13:12%253C1175::AID-RCM639%253E3.0.CO;2-0.

(9) Choi, B. K.; Gusev, A. I.; Hercules, D. M. Postcolumn Introduction of an Internal Standard for Quantitative LC−MS Analysis. *Anal. Chem.* **1999**, *71* (18), 4107–4110. https://doi.org/10.1021/ac990312o.

(10) Zhao, X.; Metcalfe, C. D. Characterizing and Compensating for Matrix Effects Using Atmospheric Pressure Chemical Ionization Liquid Chromatography−Tandem Mass Spectrometry: Analysis of Neutral Pharmaceuticals in Municipal Wastewater. *Anal. Chem.* **2008**, *80* (6), 2010–2017. https://doi.org/10.1021/ac701633m.

(11) Rossmann, J.; Gurke, R.; Renner, L. D.; Oertel, R.; Kirch, W. Evaluation of the Matrix Effect of Different Sample Matrices for 33 Pharmaceuticals by Post-Column Infusion. *Journal of Chromatography B* **2015**, *1000*, 84–94. https://doi.org/10.1016/j.jchromb.2015.06.019.

(12) Chang, K. C.; Su, J. J.; Cheng, C. Development of Online Sampling and Matrix Reduction Technique Coupled Liquid Chromatography/Ion Trap Mass Spectrometry for Determination Maduramicin in Chicken Meat. *Food Chemistry* **2013**, *141* (2), 1522–1529. https://doi.org/10.1016/j.foodchem.2013.04.016.

(13) Liao, H.-W.; Chen, G.-Y.; Tsai, I.-L.; Kuo, C.-H. Using a Postcolumn-Infused Internal Standard for Correcting the Matrix Effects of Urine Specimens in Liquid Chromatography–Electrospray Ionization Mass

Spectrometry. *Journal of Chromatography A* **2014**, *1327*, 97–104. https://doi.org/10.1016/j.chroma.2013.12.066.
(14) González, O.; Van Vliet, M.; Damen, C. W. N.; Van Der Kloet, F. M.; Vreeken, R. J.; Hankemeier, T. Matrix Effect Compensation in Small-Molecule Profiling for an LC–TOF Platform Using Multicomponent Postcolumn Infusion. *Anal. Chem.* **2015**, *87* (12), 5921–5929. https://doi.org/10.1021/ac504268y.
(15) Rossmann, J.; Renner, L. D.; Oertel, R.; El-Armouche, A. Post-Column Infusion of Internal Standard Quantification for Liquid Chromatography-Electrospray Ionization-Tandem Mass Spectrometry Analysis – Pharmaceuticals in Urine as Example Approach. *Journal of Chromatography A* **2018**, *1535*, 80–87. https://doi.org/10.1016/j.chroma.2018.01.001.
(16) Chiu, H.-H.; Liao, H.-W.; Shao, Y.-Y.; Lu, Y.-S.; Lin, C.-H.; Tsai, I.-L.; Kuo, C.-H. Development of a General Method for Quantifying IgG-Based Therapeutic Monoclonal Antibodies in Human Plasma Using Protein G Purification Coupled with a Two Internal Standard Calibration Strategy Using LC-MS/MS. *Analytica Chimica Acta* **2018**, *1019*, 93–102. https://doi.org/10.1016/j.aca.2018.02.040.
(17) Liao, H.-W.; Lin, S.-W.; Chen, G.-Y.; Kuo, C.-H. Estimation and Correction of the Blood Volume Variations of Dried Blood Spots Using a Postcolumn Infused-Internal Standard Strategy with LC-Electrospray Ionization-MS. *Anal. Chem.* **2016**, *88* (12), 6457–6464. https://doi.org/10.1021/acs.analchem.6b01145.
(18) Jhang, R.-S.; Lin, S.-Y.; Peng, Y.-F.; Chao, H.-C.; Tsai, I.-L.; Lin, Y.-T.; Liao, H.-W.; Tang, S.-C.; Kuo, C.-H.; Jeng, J.-S. Using the PCI-IS Method to Simultaneously Estimate Blood Volume and Quantify Nonvitamin K Antagonist Oral Anticoagulant Concentrations in Dried Blood Spots. *Anal. Chem.* **2020**, *92* (3), 2511–2518. https://doi.org/10.1021/acs.analchem.9b04063.
(19) Stahnke, H.; Reemtsma, T.; Alder, L. Compensation of Matrix Effects by Postcolumn Infusion of a Monitor Substance in Multiresidue Analysis with LC−MS/MS. *Anal. Chem.* **2009**, *81* (6), 2185–2192. https://doi.org/10.1021/ac802362s.
(20) Liao, H.-W.; Chen, G.-Y.; Wu, M.-S.; Liao, W.-C.; Tsai, I.-L.; Kuo, C.-H. Quantification of Endogenous Metabolites by the Postcolumn Infused-Internal Standard Method Combined with Matrix Normalization Factor in Liquid Chromatography–Electrospray Ionization Tandem Mass Spectrometry. *Journal of Chromatography A* **2015**, *1375*, 62–68. https://doi.org/10.1016/j.chroma.2014.11.073.
(21) Liao, H.-W.; Chen, G.-Y.; Wu, M.-S.; Liao, W.-C.; Lin, C.-H.; Kuo, C.-H. Development of a Postcolumn Infused-Internal Standard Liquid Chromatography Mass Spectrometry Method for Quantitative Metabolomics Studies. *J. Proteome Res.* **2017**, *16* (2), 1097–1104. https://doi.org/10.1021/acs.jproteome.6b01011.
(22) Huang, M.; Li, H.-Y.; Liao, H.-W.; Lin, C.-H.; Wang, C.-Y.; Kuo, W.-H.; Kuo, C.-H. Using Post-Column Infused Internal Standard Assisted Quantitative Metabolomics for Establishing Prediction Models for Breast Cancer Detection. *Rapid Communications in Mass Spectrometry* **2020**, *34* (S1), e8581. https://doi.org/10.1002/rcm.8581.
(23) Lo, C.; Hsu, Y.-L.; Cheng, C.-N.; Lin, C.-H.; Kuo, H.-C.; Huang, C.-S.; Kuo, C.-H. Investigating the Association of the Biogenic Amine Profile in Urine with Therapeutic Response to Neoadjuvant Chemotherapy in Breast Cancer Patients. *J. Proteome Res.* **2020**, *19* (10), 4061–4070. https://doi.org/10.1021/acs.jproteome.0c00362.
(24) Liao, H.-W.; Kuo, C.-H.; Chao, H.-C.; Chen, G.-Y. Post-Column Infused Internal Standard Assisted Lipidomics Profiling Strategy and Its Application on Phosphatidylcholine Research. *Journal of Pharmaceutical and Biomedical Analysis* **2020**, *178*, 112956. https://doi.org/10.1016/j.jpba.2019.112956.
(25) Chepyala, D.; Kuo, H.-C.; Su, K.-Y.; Liao, H.-W.; Wang, S.-Y.; Chepyala, S. R.; Chang, L.-C.; Kuo, C.-H. Improved Dried Blood Spot-Based Metabolomics Analysis by a Postcolumn Infused-Internal Standard Assisted Liquid Chromatography-Electrospray Ionization Mass Spectrometry Method. *Anal. Chem.* **2019**, *91* (16), 10702–10712. https://doi.org/10.1021/acs.analchem.9b02050.
(26) González, O.; Dubbelman, A.-C.; Hankemeier, T. Postcolumn Infusion as a Quality Control Tool for LC-MS-Based Analysis. *J. Am. Soc. Mass Spectrom.* **2022**, *33* (6), 1077–1080. https://doi.org/10.1021/jasms.2c00022.
(27) Tisler, S.; Pattison, D. I.; Christensen, J. H. Correction of Matrix Effects for Reliable Non-Target Screening LC–ESI–MS Analysis of Wastewater. *Anal. Chem.* **2021**, *93* (24), 8432–8441. https://doi.org/10.1021/acs.analchem.1c00357.
(28) Zhu, P.; Dubbelman, A.-C.; Hunter, C.; Genangeli, M.; Karu, N.; Harms, A.; Hankemeier, T. Development of an Untargeted LC-MS Metabolomics Method with Postcolumn Infusion for Matrix Effect Monitoring in Plasma and Feces. *J. Am. Soc. Mass Spectrom.* **2024**, *35* (3), 590–602. https://doi.org/10.1021/jasms.3c00418.
(29) Dubbelman, A.-C.; van Wieringen, B.; Roman Arias, L.; van Vliet, M.; Vermeulen, R.; Harms, A. C.; Hankemeier, T. Strategies for Using Postcolumn Infusion of Standards to Correct for Matrix Effect in LC-

MS-Based Quantitative Metabolomics. *J. Am. Soc. Mass Spectrom.* **2024**. https://doi.org/10.1021/jasms.4c00408.

(30) González, O.; van Vliet, M.; Damen, C. W. N.; van der Kloet, F. M.; Vreeken, R. J.; Hankemeier, T. Matrix Effect Compensation in Small-Molecule Profiling for an LC–TOF Platform Using Multicomponent Postcolumn Infusion. *Anal. Chem.* **2015**, *87* (12), 5921–5929. https://doi.org/10.1021/ac504268y.

(31) Tisler, S.; Pattison, D. I.; Christensen, J. H. Correction of Matrix Effects for Reliable Non-Target Screening LC–ESI–MS Analysis of Wastewater. *Analytical Chemistry* **2021**, acs.analchem.1c00357. https://doi.org/10.1021/acs.analchem.1c00357.

(32) Rožman, M. Proton Affinity of Several Basic Non-Standard Amino Acids. *Chemical Physics Letters* **2012**, *543*, 50–54. https://doi.org/10.1016/j.cplett.2012.06.048.

(33) Rundlett, K. L.; Armstrong, D. W. Mechanism of Signal Suppression by Anionic Surfactants in Capillary Electrophoresis−Electrospray Ionization Mass Spectrometry. *Anal. Chem.* **1996**, *68* (19), 3493–3497. https://doi.org/10.1021/ac960472p.

(34) Evans, A. M.; O'Donovan, C.; Playdon, M.; Beecher, C.; Beger, R. D.; Bowden, J. A.; Broadhurst, D.; Clish, C. B.; Dasari, S.; Dunn, W. B.; Griffin, J. L.; Hartung, T.; Hsu, P.-C.; Huan, T.; Jans, J.; Jones, C. M.; Kachman, M.; Kleensang, A.; Lewis, M. R.; Monge, M. E.; Mosley, J. D.; Taylor, E.; Tayyari, F.; Theodoridis, G.; Torta, F.; Ubhi, B. K.; Vuckovic, D.; on behalf of the Metabolomics Quality Assurance, Q. C. C. (mQACC). Dissemination and Analysis of the Quality Assurance (QA) and Quality Control (QC) Practices of LC–MS Based Untargeted Metabolomics Practitioners. *Metabolomics* **2020**, *16* (10), 113. https://doi.org/10.1007/s11306-020-01728-5.

Supplementary Material

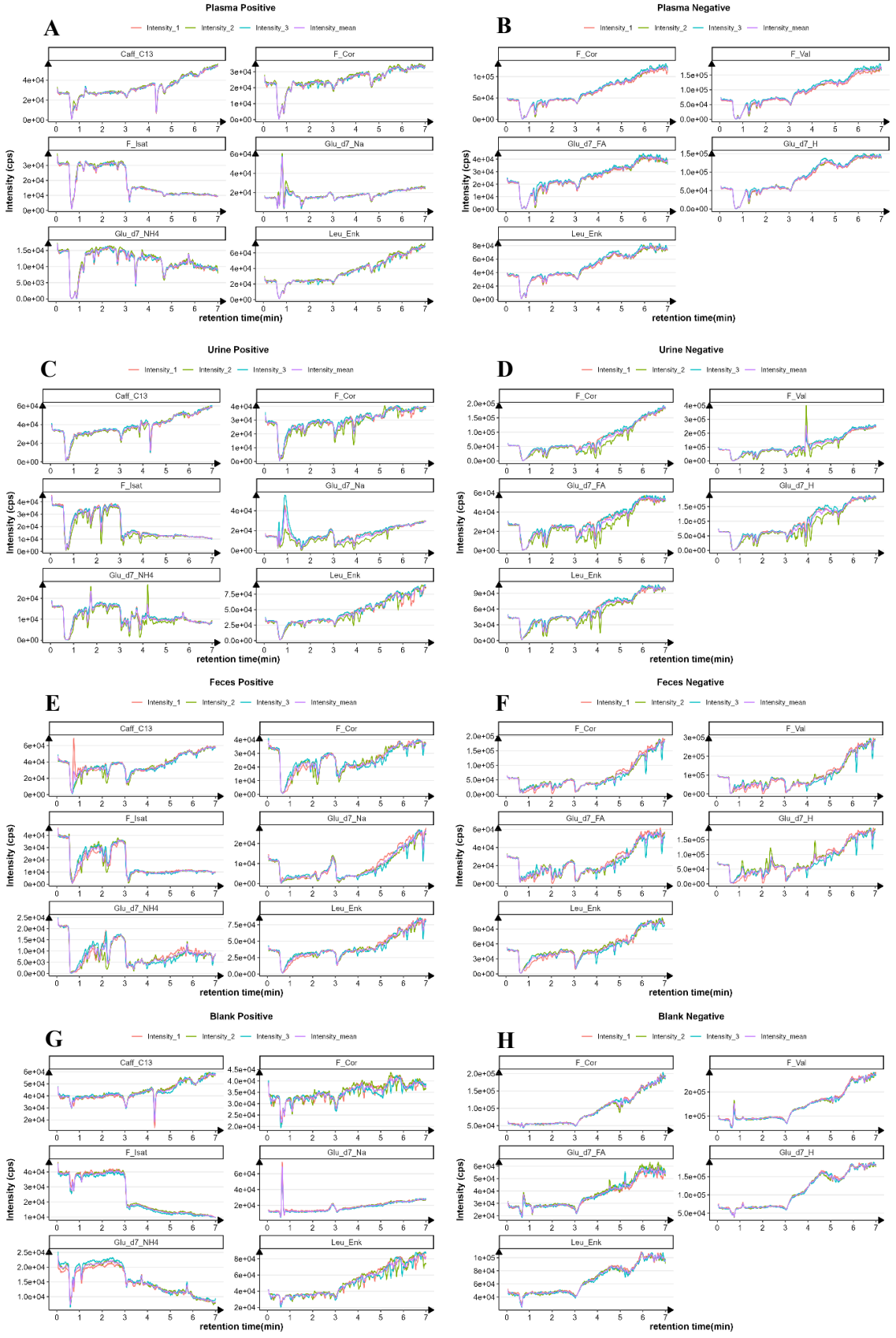

Figure S1. Infusion profiles for 0-7 minutes all PCISs with injections of plasma (A, B), urine (C, D), feces (E,F) and solvent blanks (G, H) in positive and negative modes. Three replicates are plotted for solvent blanks; samples from three different individuals are plotted for plasma, urine, and feces

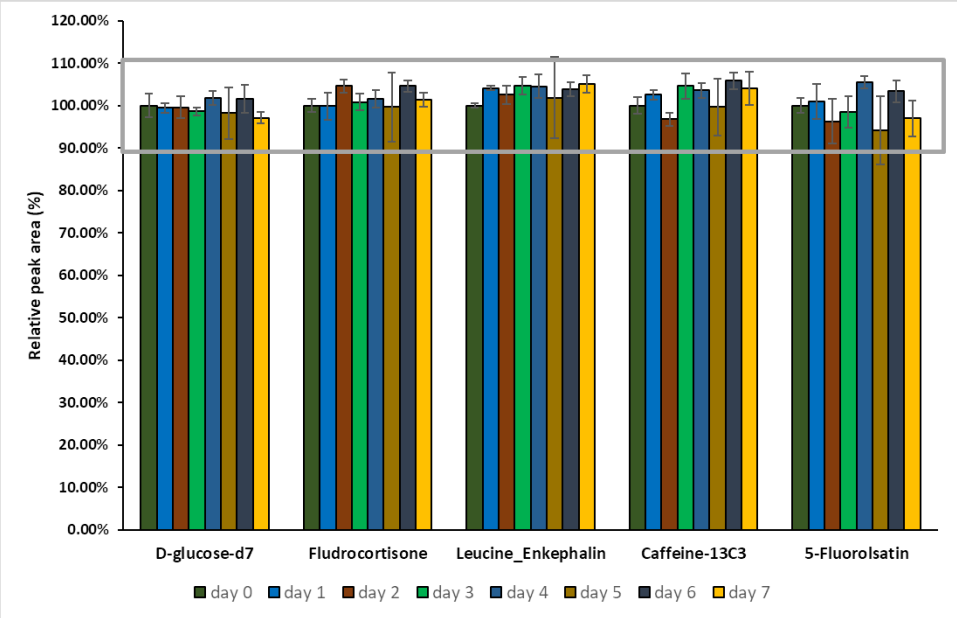

Figure S2. Seven-days room temperature stability test for all the selected PCISs, except for 3-fluoro-DL-valine.

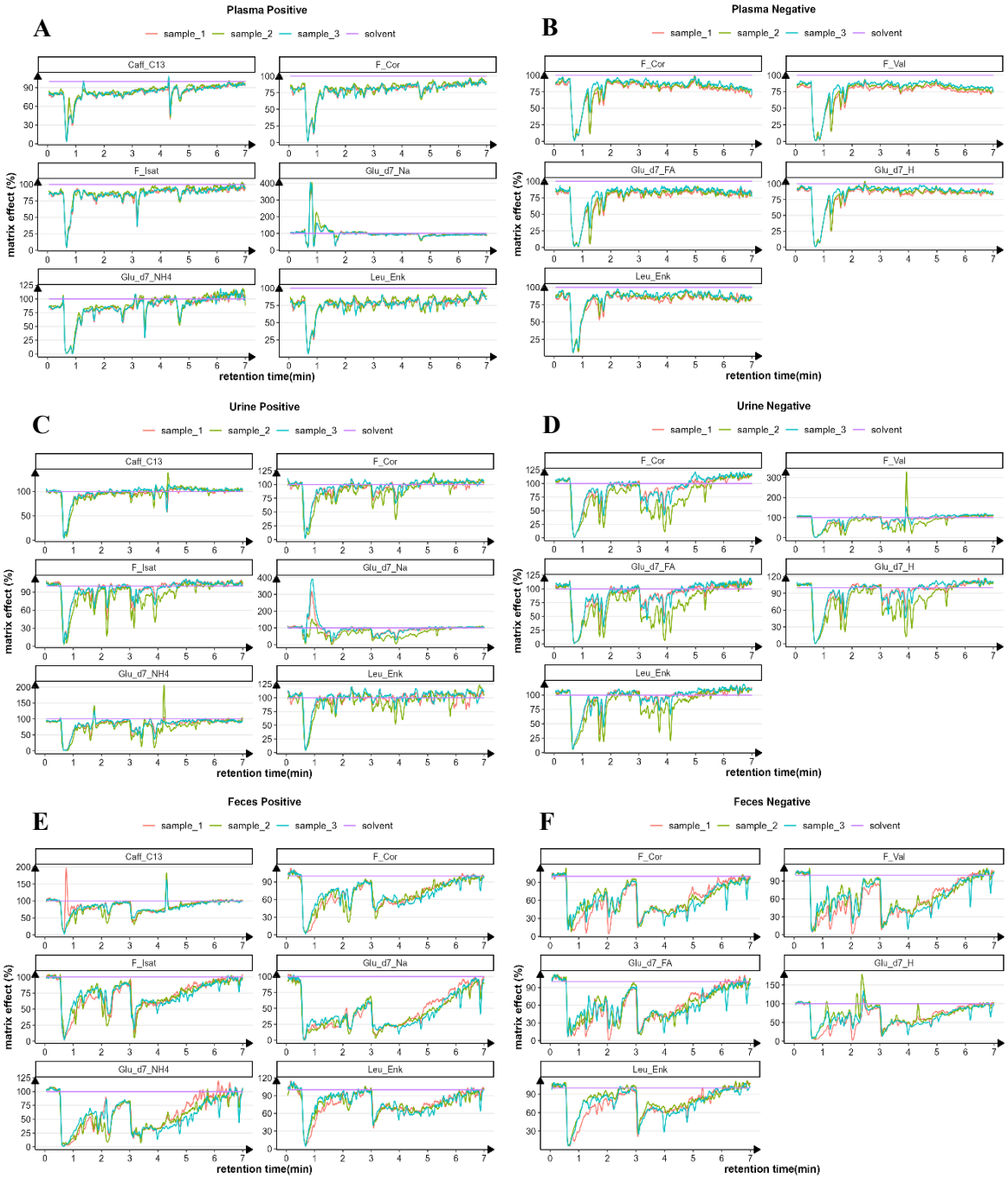

Figure S3. Matrix effect profiles from 0-7 minutes for all PCISs monitored in plasma (A, B), urine (C, D), and fecal samples (E, F) in positive and negative modes. For each ionization mode and PCIS, the averaged intensity of the infusion profile from three solvent samples was used as the reference (100% matrix effect).

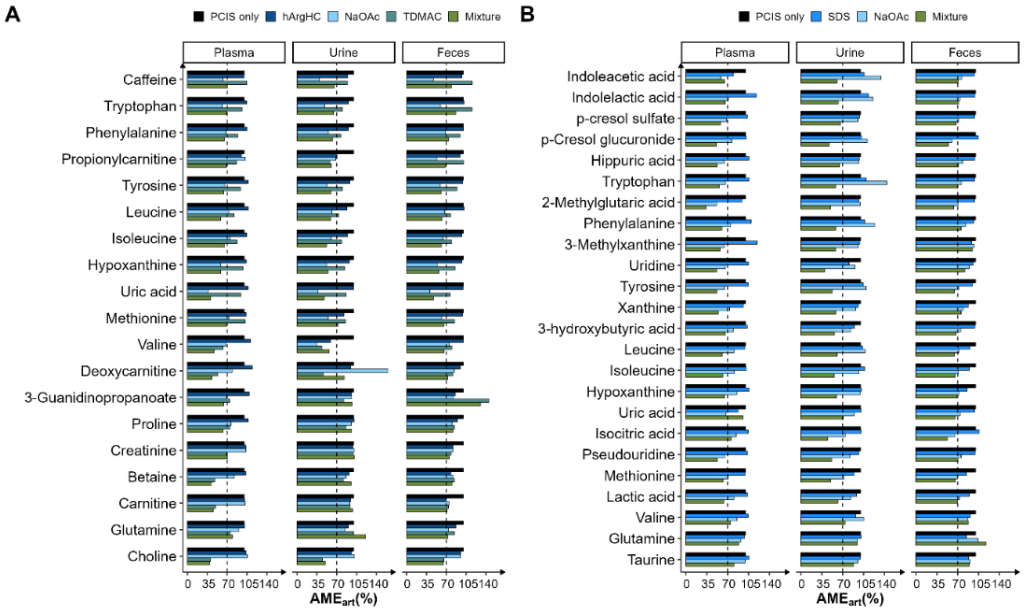

Figure S4. MEart induced by individual artificial matrix compounds and the mixture of all artificial matrix compounds (Mixture) in positive (A) and negative (B) modes for plasma, urine, and feces, across all examined metabolites. "PCIS only" is used as a reference with no induced ME_{art} (MEart = 100%), and the dashed line indicates 70% of ME_{art}.

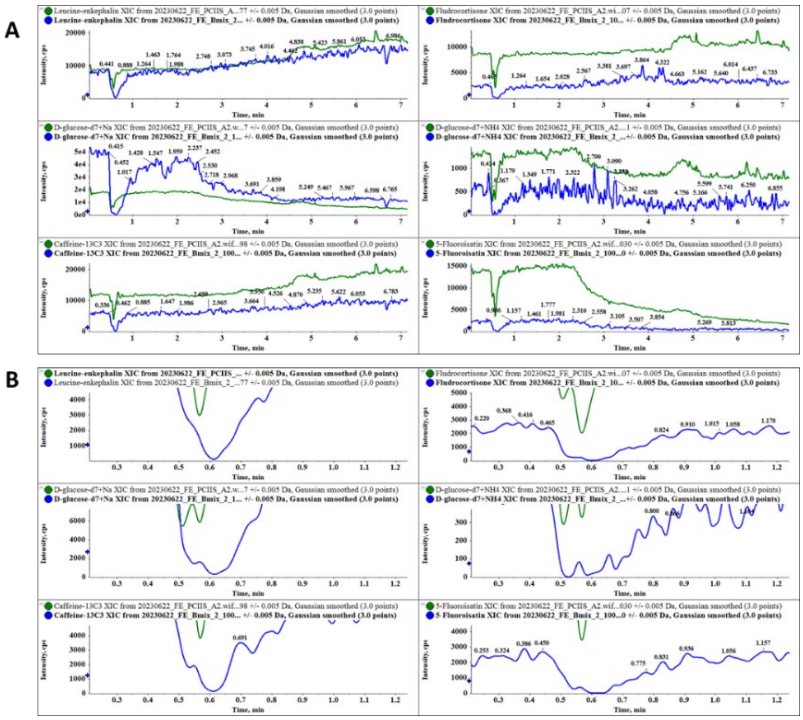

Figure S5. Infusion profiles of PCIS (A) and zoomed-in plots of the region with severe suppression (B) for a pooled fecal sample with infusion of PCIS (green line) and PCIS plus the mixture of artificial matrix compounds (blue line) in positive mode.

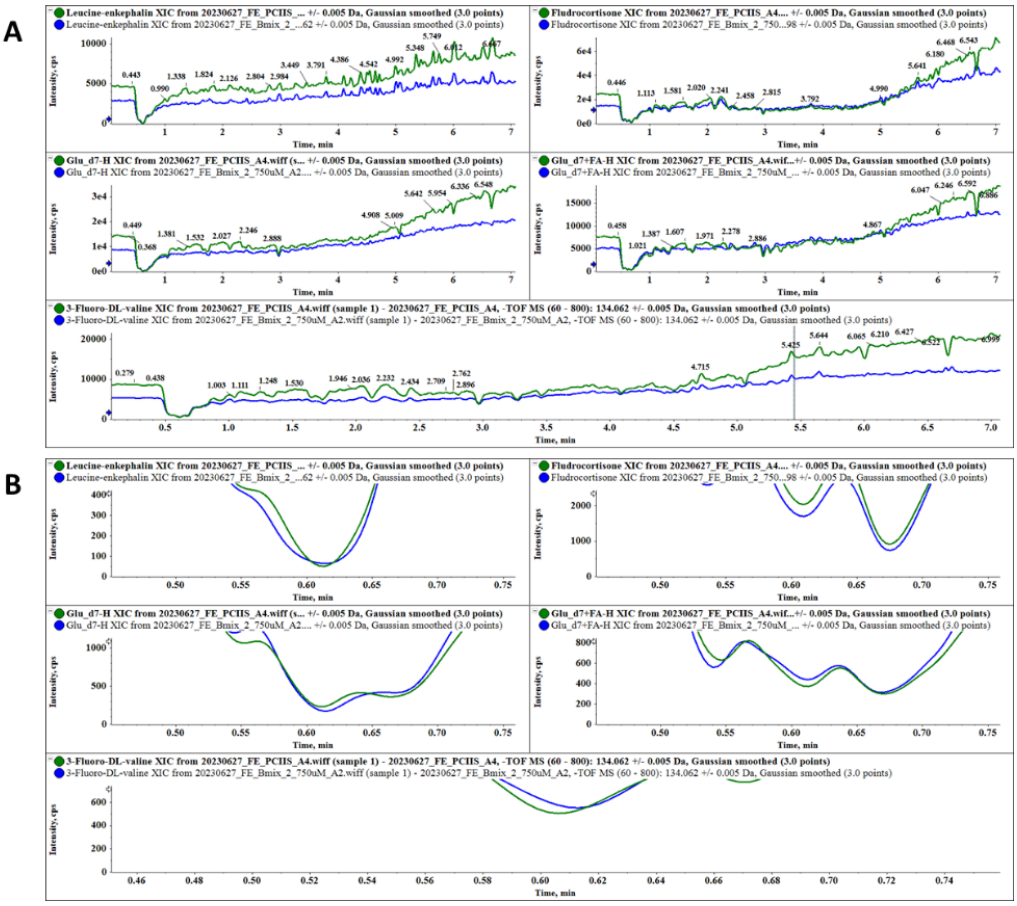

Figure S6. Infusion profiles of PCISs (A) and zoomed-in plots of the region with severe suppression (B) for a pooled fecal sample with infusion of PCIS (green line) and PCIS plus the mixture of artificial matrix compounds (blue line) in negative mode.

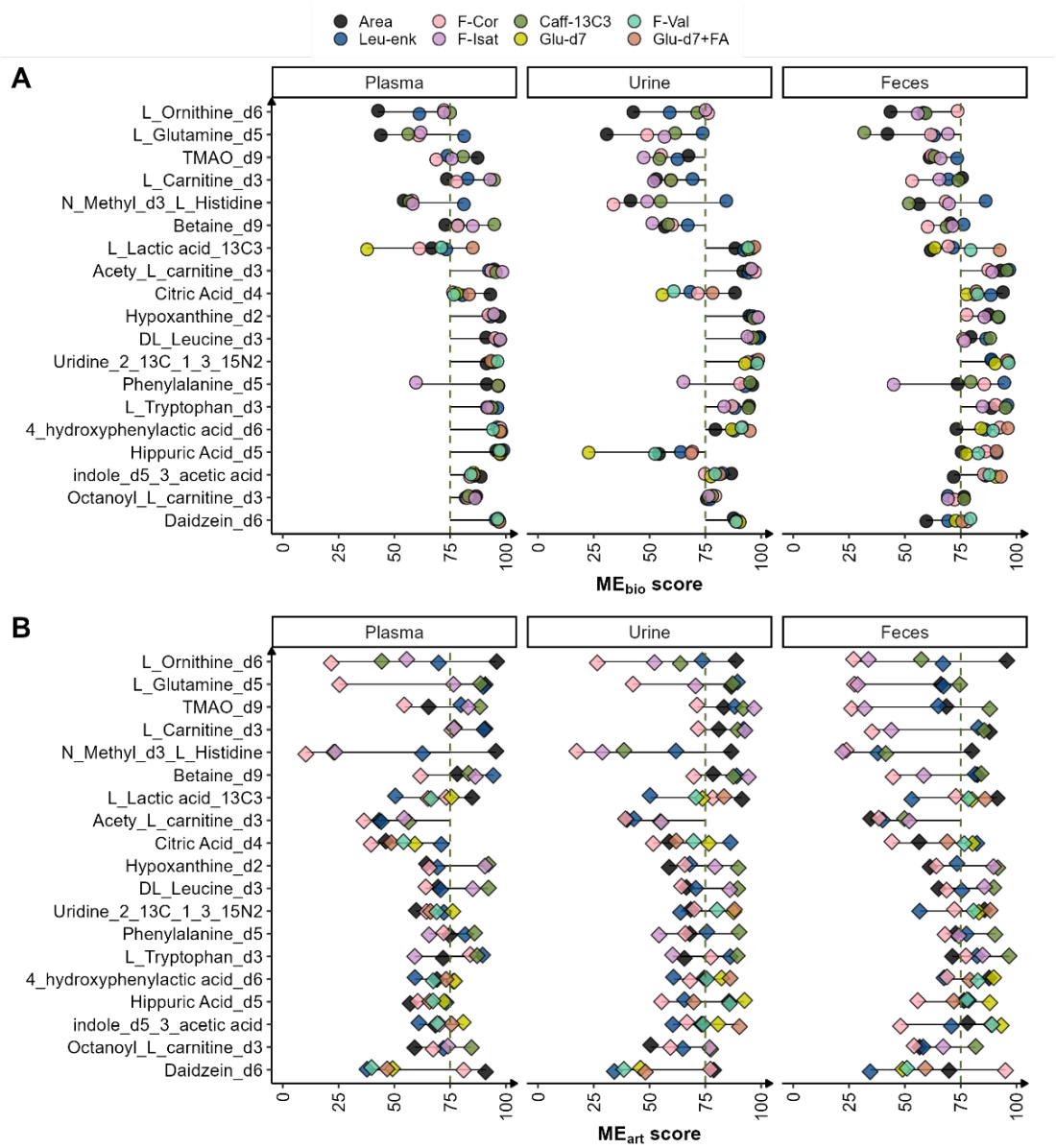

Figure S7. The ME_{bio} (A) and ME_{art} (B) scores of 19 SIL standards spiked in plasma, urine and feces before and after PCIS correction.

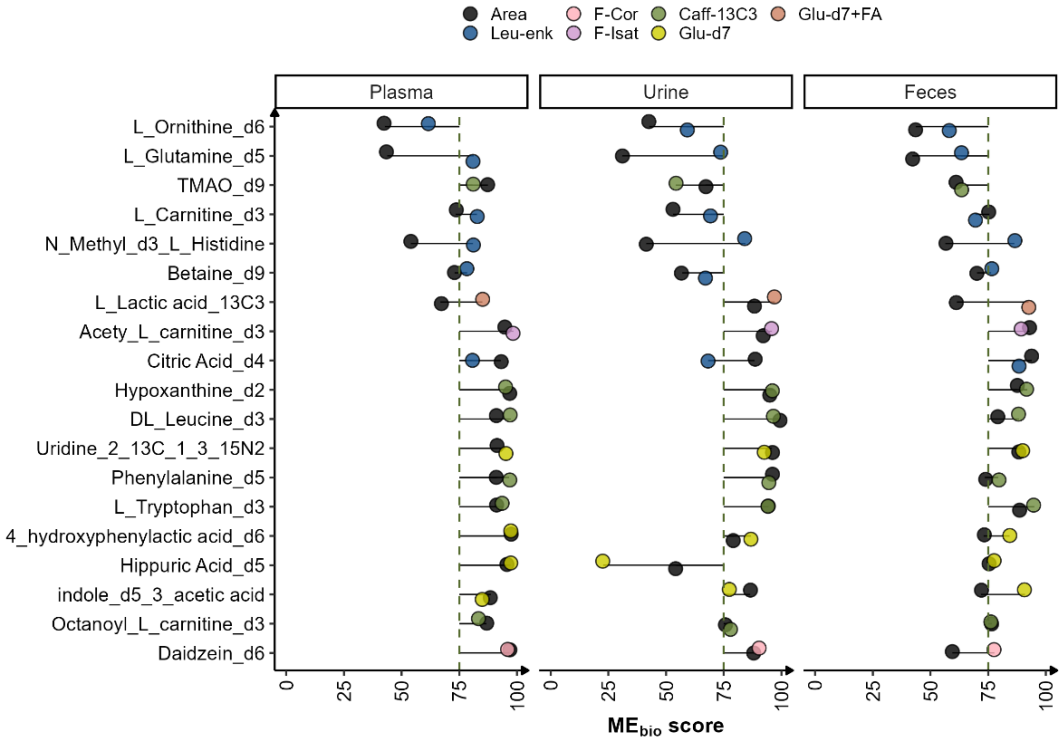

Figure S8. The ME_{bio} score of the 19 SIL standards spiked in plasma, urine and feces before and after correction with the PCIS selected with artificial matrix infusion. The dashed line indicates an ME_{bio} score of 75.

Table S1: General information and stock solution preparation for all the authentic standards

Compound Name	Compound Formula	Monoisotopic Mass/Da	CAS number	supplier	stock /mM	Solvent	usage
L-ornithine-d_6	C3D9NO	84.1249	347841-40-1	CDN	250.0	H2O	SIL
L-glutamine-d_5	C5H5D5N2O3	151.1005	14341-78-7	cambridge Isotope laboratories	250.0	H2O (1% NH3.H2O)	SIL
TMAO-d_9	C3D9NO	84.1249	1161070-49-0	cambridge Isotope laboratories	500.0	H2O	SIL
L-carnitine-d_3	C7H12D3NO3	164.1240	350818-62-1	CDN	125.0	H2O	SIL
n-methyl-d_3-l-histidine	C7D3H9N3O2	172.1040	91037-48-8	CDN	25.0	H2O	SIL
Betaine-d_9	C5H2D9NO2	126.1355	285979-85-3	CDN	250.0	H2O	SIL
L-lactic acid-$^{13}C_3$	13C3H6O3	93.0418	201595-71-3	TRC	170.0	H2O	SIL
acety-L-carnitine-d_3	C9H14D3NO4	206.1346	1334532-17-0	CDN	50.0	H2O	SIL
citric acid-d_4	C6H4D4O7	196.0521	147664-83-3	cambridge Isotope laboratories	1250.0	H2O	SIL
hypoxanthine-d_2	C5D3HN4O	140.0636	NA	cambridge Isotope laboratories	62.5	10% MeOH (0.2M HCL)	SIL
DL-leucine-d3	C6H10D3NO2	134.1135	87828-86-2	CDN	62.5	10% MeOH (1% NH3.H2O)	SIL
uridine-2-^{13}C-1,3-$^{15}N_2$	C8[13C]1H12[15N]2O6	247.0670	369656-75-7	TRC	31.3	H2O	SIL

phenylalanine-d_5	C9H6D5NO2	170.1104	28466-89-7	CDN	50.0	15% MeOH	SIL
L-tryptophan-d_3	C11H9D3N2O2	207.1087	133519-78-5	CDN	50.0	H2O (0.5% NH3.H2O)	SIL
4-hydroxyphenylactic acid-d_6	C8H2D6O3	158.0850	100287-06-7	TRC	125.0	H2O (1.5% NH3.H2O)	SIL
hippuric acid-d_5	C9H4D5NO3	184.0896	53518-98-2	chem Cruz	12.5	H2O	SIL
indole-d_5-3-acetic acid	C10H4D5NO2	180.0947	76937-78-5	TRC	1.3	MeOH	SIL
daidzein-d_6	C15H4D6O4	260.0956	291759-05-2	TRC	0.1	MeOH	SIL
octanoyl-l-carnitine-d_3	C15H26D3NO4	290.2285	1334532-24-9	CDN	2.5	H2O	SIL
leucine-enkephalin	C28H37N5O7	555.2693	81678-16-2	Sigma-Aldrich	1.8	H2O	PCIS
fludrocortisone	C21H29FO5	380.1999	127-31-1	TRC	1.3	MeOH	PCIS
5-fluoroisatin	C8H4FNO2	165.0226	443-69-6	Sigma-Aldrich	6.1	50% MeOH	PCIS
caffeine-$^{13}C_3$	C5[13C]3H10N4O2	197.0904	78072-66-9	TRC	2.5	50% MeOH	PCIS
3-fluoro-DL-valine	C5H10FNO2	135.0696	43163-94-6	Sigma-Aldrich	14.8	50% MeOH	PCIS
L-homoarginine hydrochloride	C7H17ClN4O2	224.1040	1483-01-8	sigma	3.0	50% ACN	artificial matrix compound
sodium dodecyl sulphate	NaSO4C12H25	288.1371	151-21-3	J.T. Baker	1.5	50% ACN	artificial matrix compound
sodium acetate	C2H3NaO2	82.0031	127-09-3	Alfa Aesar	100.0	20% ACN	artificial matrix compound
tridodecylmethylammonium chloride	C37H78ClN	571.5823	7173-54-8	Fluka	1.5	50% ACN	artificial matrix compound

Table S2: Retention time, detection polarity, and final concentrations in the biological samples after post-extration spiking of all the SIL standards

SIL standards	ME_{bio} calculation		ME_{art} calculation (uM)	Retention time/min in Triple TOF 6600 system	Retention time/min in Triple TOF 5600 system	Polarity for detection
	low (uM)	high (uM)				
L-ornithine-d_6	60.0	600.0	300	0.57	0.56	Positive
L-glutamine-d_5	600.0	6000.0	300	0.66	0.66	Positive
TMAO-d_9	40.0	400.0	40	0.69	0.69	Positive
L-carnitine-d_3	30.0	300.0	10	0.69	0.69	Positive
n-methyl-d_3-l-histidine	3.0	30.0	75	0.70	0.70	Positive
Betaine-d_9	50.0	500.0	10	0.71	0.71	Positive
L-lactic acid-$^{13}C_3$	150.0	1500.0	75	1.25	1.20	Negative
acety-L-carnitine-d_3	5.0	50.0	2.5	1.40	1.27	Positive
citric acid-d_4	100.0	1000.0	50	1.57	1.57	Negative
hypoxanthine-d_2	5.0	50.0	25	1.83	1.75	Positive
DL-leucine-d3	80.0	800.0	40	2.42	2.19	Positive
uridine-2-^{13}C-1,3-$^{15}N_2$	5.0	50.0	25	2.72	2.44	Negative
phenylalanine-d_5	80.0	800.0	16	3.06	3.03	Positive
L-tryptophan-d_3	80.0	800.0	40	3.32	3.55	Positive
4-hydroxyphenylactic acid-d_6	1.0	10.0	10	3.79	4.07	Negative
hippuric acid-d_5	5.0	50.0	10	3.86	4.13	Negative
indole-d_5-3-acetic acid	1.0	10.0	50	4.73	5.14	Negative
daidzein-d_6	0.5	5.0	2.5	4.80	5.28	Negative
octanoyl-l-carnitine-d_3	0.2	2.0	1	4.86	5.22	Positive

Table S3: structures overview of PCIS candidates

Standards name	Molecular structure	Polarity assessed
Leucine-enkephalin	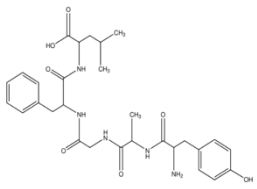	positive and negative
Fludrocortisone	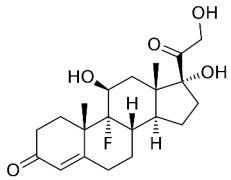	positive and negative
D-glucose-d_7	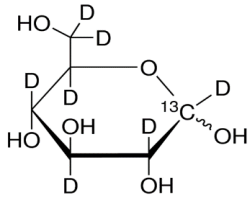	positive and negative
5-Fluoroisatin	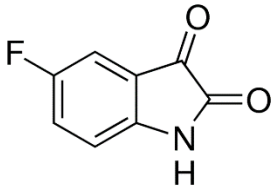	positive and negative
Caffeine-$^{13}C3$	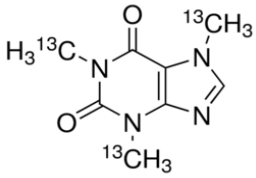	positive
3-Fluoro-DL-valine	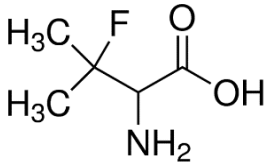	positive and negative

Table S4: Pearson correlation coeffecient (r) of the infusion profiles between PCIS candidates in diverse plasma samples (positive ionization mode)

Sanquine Plasma	[D-glucose-d_7 + Na]+	[Fludrocortisone +H]+	[Leucine-enkepahlin +H]+	[Caffeine$^{13}C_3$ +H]+	[3-Fluoro-DL-valine+H]+	[5-Fluorosatin+H]+
[D-glucose-d_7 + Na]+	1					
[Fludrocortisone +H]+	0.770804431	1				
[Leucine-enkepahlin +H]+	0.772241398	0.824544	1			
[Caffeine$^{13}C_3$ +H]+	0.807158021	0.880798384	0.905081916	1		
[3-Fluoro-DL-valine+H]+	0.72848998	0.735984463	0.968348889	0.894836281	1	
[5-Fluorosatin+H]+	-0.200570801	-0.01464634	-0.532458303	-0.246552806	-0.575077475	1

Divbiosc Plasma	[D-glucose-d_7 + Na]+	[Fludrocortisone +H]+	[Leucine-enkepahlin +H]+	[Caffeine$^{13}C_3$ +H]+	[3-Fluoro-DL-valine+H]+	[5-Fluorosatin+H]+
[D-glucose-d_7 + Na]+	1					
[Fludrocortisone +H]+	0.630635012	1				
[Leucine-enkepahlin +H]+	0.694528207	0.834120488	1			
[Caffeine$^{13}C_3$ +H]+	0.683401118	0.868356752	0.901571591	1		
[3-Fluoro-DL-valine+H]+	0.538261395	0.705531452	0.921834288	0.877180876	1	
[5-Fluorosatin+H]+	-0.190154901	-0.031721979	-0.526404679	-0.283939985	-0.606670633	1

Fasting Plasma	[D-glucose-d_7 + Na]+	[Fludrocortisone +H]+	[Leucine-enkepahlin +H]+	[Caffeine$^{13}C_3$ +H]+	[3-Fluoro-DL-valine+H]+	[5-Fluorosatin+H]+
[D-glucose-d_7 + Na]+	1					
[Fludrocortisone +H]+	0.683430579	1				
[Leucine-enkepahlin +H]+	0.703838424	0.828812768	1			
[Caffeine$^{13}C_3$ +H]+	0.740523259	0.867595416	0.899915573	1		
[3-Fluoro-DL-valine+H]+	0.663754647	0.73810718	0.968591541	0.897303108	1	
[5-Fluorosatin+H]+	-0.256899697	-0.06528373	-0.572740147	-0.304372961	-0.616763643	1

Non-fasting Plasma	[D-glucose-d_7 + Na]+	[Fludrocortisone +H]+	[Leucine-enkepahlin +H]+	[Caffeine$^{13}C_3$ +H]+	[3-Fluoro-DL-valine+H]+	[5-Fluorosatin+H]+
[D-glucose-d_7 + Na]+	1					
[Fludrocortisone +H]+	0.647767404	1				
[Leucine-enkepahlin +H]+	0.653235124	0.792877554	1			
[Caffeine$^{13}C_3$ +H]+	0.70200815	0.813079254	0.890842094	1		
[3-Fluoro-DL-valine+H]+	0.587276227	0.681877501	0.965422476	0.882096272	1	
[5-Fluorosatin+H]+	-0.161839449	-0.019331194	-0.564482804	-0.310651998	-0.626161036	1

Table S5: Pearson correlation coeffecient (r) of the infusion profiles between PCIS candidates in diverse plasma samples (negative ionization mode)

Sanquine Plasma	[D-glucose-d_7 -H]-	[Fludrocortisone+FA-H]-	[Leucine-enkepahlin -H]-	[3-Fluoro-DL-valine-H]-	[5-Fluoroisatin-H]-
[D-glucose-d_7 -H]-	1				
[Fludrocortisone+FA-H]-	0.971665897	1			
[Leucine-enkepahlin -H]-	0.913084057	0.877045789	1		
[3-Fluoro-DL-valine-H]-	0.985792414	0.97978939	0.904547957	1	
[5-Fluoroisatin-H]-	0.931715540	0.894316261	0.992686476	0.917705787	1

Divbiosc Plasma	[D-glucose-d_7 -H]-	[Fludrocortisone+FA-H]-	[Leucine-enkepahlin -H]-	[3-Fluoro-DL-valine-H]-	[5-Fluoroisatin-H]-
[D-glucose-d_7 -H]-	1				
[Fludrocortisone+FA-H]-	0.981822481	1			
[Leucine-enkepahlin -H]-	0.962978629	0.952940878	1		
[3-Fluoro-DL-valine-H]-	0.9891261	0.98361744	0.959161467	1	
[5-Fluoroisatin-H]-	0.964913125	0.956276829	0.994226765	0.953515605	1

Fasting Plasma	[D-glucose-d_7 -H]-	[Fludrocortisone+FA-H]-	[Leucine-enkepahlin -H]-	[3-Fluoro-DL-valine-H]-	[5-Fluoroisatin-H]-
[D-glucose-d_7 -H]-	1				
[Fludrocortisone+FA-H]-	0.981660938	1			
[Leucine-enkepahlin -H]-	0.947698008	0.921857285	1		
[3-Fluoro-DL-valine-H]-	0.984958237	0.982635835	0.933553917	1	
[5-Fluoroisatin-H]-	0.960629360	0.940410637	0.99140311	0.941998665	1

Non-fasting Plasma	[D-glucose-d_7 -H]-	[Fludrocortisone+FA-H]-	[Leucine-enkepahlin -H]-	[3-Fluoro-DL-valine-H]-	[5-Fluoroisatin-H]-
[D-glucose-d_7 -H]-	1				
[Fludrocortisone+FA-H]-	0.984870223	1			
[Leucine-enkepahlin -H]-	0.94116293	0.918152598	1		
[3-Fluoro-DL-valine-H]-	0.98722257	0.983336006	0.928348359	1	
[5-Fluoroisatin-H]-	0.957162007	0.93747786	0.991424244	0.937538212	1

Table S6: Endogenous metabolites used for peak area comparison in plasam injections with and without PCIS infusion

Index	HMDB_ID	Metabolite_Name	Formula	MS.ready.monoiso-topic.mass	RT	Polarity	change in per-centage (%)*
1	HMDB0000378	2-Methyl-butyroylcarnitine	C12H23NO4	245.1627	3.565	Positive	-31.2
2	HMDB0013324	2-Octenoylcarnitine	C15H27NO4	285.194	4.727	Positive	-27.2
3	HMDB0000043	Betaine	C5H11NO2	117.079	0.699	Positive	-1.0
4	HMDB0000097	Choline	C5H13NO	103.0997	0.643	Positive	-0.7
5	HMDB0001161	Deoxycarnitine	C7H15NO2	145.1103	0.748	Positive	23.6
6	HMDB0000705	Hexanoylcarnitine	C13H25NO4	259.1784	4.166	Positive	-26.0
7	HMDB0002013	Isobutyrylcarnitine	C11H21NO4	231.1471	3.135	Positive	-18.4
8	HMDB0000201	Acetylcarnitine	C9H17NO4	203.1158	1.416	Positive	-7.7
9	HMDB0002250	Lauroylcarnitine	C19H37NO4	343.2723	5.89	Positive	25.4
10	HMDB0000062	Carnitine	C7H15NO3	161.1052	0.689	Positive	-9.6
11	HMDB0000791	Octanoylcarnitine	C15H29NO4	287.2097	4.855	Positive	-29.4
12	HMDB0005066	Myristoylcarnitine	C21H41NO4	371.3036	6.371	Positive	11.0
13	HMDB0000824	Propionylcarnitine	C10H19NO4	217.1314	2.963	Positive	-22.8
14	HMDB0002366	Tiglylcarnitine	C12H21NO4	243.1471	3.446	Positive	-24.0
15	HMDB0000925	TMAO	C3H9NO	75.06841	0.685	Positive	-22.9
16	HMDB0000641	Glutamine	C5H10N2O3	146.0691	0.654	Positive	-20.5
17	HMDB0000172	Isoleucine	C6H13NO2	131.0946	2.25	Positive	12.6
18	HMDB0000684	Kynurenine	C10H12N2O3	208.0848	3.059	Positive	-14.0
19	HMDB0000687	Leucine	C6H13NO2	131.0946	2.42	Positive	20.3
20	HMDB0000696	Methionine	C5H11NO2S	149.051	1.353	Positive	1.8
21	HMDB0000214	Ornithine	C5H12N2O2	132.0899	0.568	Positive	3.9
22	HMDB0000159	Phenylalanine	C9H11NO2	165.079	3.061	Positive	-10.7
23	HMDB0000162	Proline	C5H9NO2	115.0633	0.787	Positive	24.1
24	HMDB0000929	Tryptophan	C11H12N2O2	204.0899	3.317	Positive	-2.0
25	HMDB0000158	Tyrosine	C9H11NO3	181.0739	2.41	Positive	29.5
26	HMDB0000883	Valine	C5H11NO2	117.079	1.082	Positive	9.4
27	HMDB0002825	Theobromine	C7H8N4O2	180.0647	3.112	Positive	-25.7
28	HMDB0000357	3-hydroxybutyric acid	C4H8O3	104.0473	2.38	Positive	1.3
29	HMDB0000619	CA	C24H40O5	408.2876	5.98	Positive	20.8
30	HMDB0000562	Creatinine	C4H7N3O	113.0589	0.737	Positive	-8.3
31	HMDB0000626	DCA	C24H40O4	392.2927	6.867	Positive	21.9
32	HMDB0000714	Hippuric acid	C9H9NO3	179.0582	3.863	Positive	2.3
33	HMDB0000197	Indoleacetic acid	C10H9NO2	175.0633	4.733	Positive	-2.1
34	HMDB0000715	Kynurenic acid	C10H7NO3	189.0426	3.457	Positive	-16.9

35	HMDB0000036	TCA	C26H45NO7S	515.2917	5.126	Positive	-32.8
36	HMDB0000289	Uric acid	C5H4N4O3	168.0283	1.692	Positive	-16.4
37	HMDB0000292	Xanthine	C5H4N4O2	152.0334	2.268	Positive	-25.8
38	HMDB0000422	2-MethylglutaricÂ acid	C6H10O4	146.0579	3.371	Positive	-27.8
39	HMDB0000157	Hypoxanthine	C5H4N4O	136.0385	1.83	Positive	-31.7
40	HMDB0002302	Indolepropionic acid	C11H11NO2	189.079	5.08	Positive	-1.0
41	HMDB0000262	Thymine	C5H6N2O2	126.0429	2.96	Positive	-22.0
42	HMDB0000301	Urocanic acid	C6H6N2O2	138.0429	1.5	Positive	-14.2
43	HMDB0000906	Trimethylamine (TMA)	C3H9N	59.0735	0.654	Positive	3.0
44	HMDB0001886	3-methylxanthine	C6H6N4O2	166.0491	3	Positive	-11.8
45	HMDB0013222	3-Guanidinopropano-ate	C4H9N3O2	131.0695	0.825	Positive	-3.2
46	HMDB0004824	N2.N2-dimethylguano-sine	C12H17N5O5	311.123	3.05	Positive	27.9
47	HMDB0000767	Pseudouridine	C9H12N2O6	244.0695	1.35	Positive	-9.8
48	HMDB0001847	Caffeine	C8H10N4O2	194.0804	3.67	Positive	-25.5
49	HMDB0000671	Indolelactic acid	C11H11NO3	205.0739	4.42	Positive	-7.2
50	HMDB0000842	Quinaldic acid	C10H7NO2	173.0477	3.63	Positive	2.2
51	HMDB0005862	2-Methylguanosine	C11H15N5O5	297.1073	2.94	Positive	1.4
52	HMDB0011621	Cinnamoylglycine	C11H11NO3	205.0739	4.53	Positive	-7.2
53	HMDB0000631	GDCA	C26H43NO5	449.3141	6.12	Positive	-3.8
54	HMDB0000698	GLCA	C26H43NO4	433.3192	6.85	Positive	-6.5
55	HMDB0000896	TDCA	C26H45NO6S	499.2968	5.72	Positive	-22.1
56	HMDB0000637	GCDCA	C26H43NO5	449.3141	6.01	Positive	-6.5
57	HMDB0000138	GCA	C26H43NO6	465.309	5.44	Positive	-21.0
58	HMDB0000951	TCDCA	C26H45NO6S	499.2968	5.59	Positive	-28.2
59	HMDB0000708	GUDCA	C26H43NO5	449.3141	5.47	Positive	-19.1
60	HMDB0000518	CDCA	C24H40O4	392.2927	6.73	Positive	23.2
61	HMDB0000641	Glutamine	C5H10N2O3	146.0691	0.66	Negative	-36.1
62	HMDB0000172	Isoleucine	C6H13NO2	131.0946	2.26	Negative	-38.4
63	HMDB0000684	Kynurenine	C10H12N2O3	208.0848	3.05	Negative	-7.9
64	HMDB0000687	Leucine	C6H13NO2	131.0946	2.44	Negative	-34.8
65	HMDB0000696	Methionine	C5H11NO2S	149.051	1.35	Negative	-10.3
66	HMDB0000159	Phenylalanine	C9H11NO2	165.079	3.06	Negative	-52.1
67	HMDB0000162	Proline	C5H9NO2	115.0633	0.78	Negative	-47.2
68	HMDB0000251	Taurine	C2H7NO3S	125.0147	0.64	Negative	-17.2
69	HMDB0000158	Tyrosine	C9H11NO3	181.0739	2.41	Negative	-49.4
70	HMDB0000883	Valine	C5H11NO2	117.079	1.08	Negative	-44.6

71	HMDB0002825	Theobromine	C7H8N4O2	180.0647	3.15	Negative	-26.8
72	HMDB0000357	3-hydroxybutyric acid	C4H8O3	104.0473	2.38	Negative	-16.1
73	HMDB0000714	Hippuric acid	C9H9NO3	179.0582	3.87	Negative	-11.5
74	HMDB0000197	Indoleacetic acid	C10H9NO2	175.0633	4.74	Negative	-47.5
75	HMDB0000715	Kynurenic acid	C10H7NO3	189.0426	3.46	Negative	-34.0
76	HMDB0000289	Uric acid	C5H4N4O3	168.0283	1.7	Negative	-19.7
77	HMDB0000292	Xanthine	C5H4N4O2	152.0334	2.27	Negative	-5.1
78	HMDB0000422	2-MethylglutaricÂ acid	C6H10O4	146.0579	3.371	Negative	4.5
79	HMDB0000157	Hypoxanthine	C5H4N4O	136.0385	1.83	Negative	-22.6
80	HMDB0000190	Lactic acid	C3H6O3	90.0317	1.25	Negative	-11.0
81	HMDB0001886	3-methylxanthine	C6H6N4O2	166.0491	3.00	Negative	9.0
82	HMDB0013222	3-Guanidinopropano-ate	C4H9N3O2	131.0695	0.83	Negative	-48.8
83	HMDB0004824	N2.N2-dimethylguano-sine	C12H17N5O5	311.123	3.05	Negative	-45.9
84	HMDB0011635	p-cresol sulfate	C7H8O4S	188.0143	4.16	Negative	-9.0
85	HMDB0000767	Pseudouridine	C9H12N2O6	244.0695	1.35	Negative	-8.9
86	HMDB0000296	Uridine	C9H12N2O6	244.0695	2.72	Negative	-30.9
87	HMDB0000671	Indolelactic acid	C11H11NO3	205.0739	4.41	Negative	-18.4
88	HMDB0011686	p-Cresol glucuronide	C13H16O7	284.0896	4.12	Negative	-36.1
89	HMDB0005862	2-Methylguanosine	C11H15N5O5	297.1073	2.95	Negative	-50.5
90	HMDB0011621	Cinnamoylglycine	C11H11NO3	205.0739	4.53	Negative	-18.4
91	HMDB0000631	GDCA	C26H43NO5	449.3141	6.12	Negative	-20.1
92	HMDB0000896	TDCA	C26H45NO6S	499.2968	5.73	Negative	-10.9
93	HMDB0000637	GCDCA	C26H43NO5	449.3141	6.01	Negative	-38.1
94	HMDB0000138	GCA	C26H43NO6	465.309	5.43	Negative	-38.1
95	HMDB0000951	TCDCA	C26H45NO6S	499.2968	5.59	Negative	-18.4
96	HMDB0000708	GUDCA	C26H43NO5	449.3141	5.46	Negative	-38.3

* change in percentage is calculated as ($A_{\text{with PCIS}}$ - $A_{\text{without PCIS}}$)/$A_{\text{without PCIS}}$ *100; A stands for peak area